

FINAL PROJECT REPORT

NASA's BIG Idea Challenge Lunar Forge: Producing Metal Products on the Moon

Production of Steel from Lunar Regolith through Carbonyl Iron Refining (CIR)

● Team Members

Collin T. Andersen, graduate student in Materials Science & Eng., team leader
John F. Otero, graduate student in Metallurgical Eng., co-team leader and foreign national (Chile)
Olivia Dale, graduate student in Metallurgical Eng., team member
Christian Norman, undergraduate student in Metallurgical Eng., team member
Cole Walker, undergraduate student in Materials Science & Eng., team member
Jason Sheets, undergraduate student in Metallurgical Eng., team member
Talon Townsend, undergraduate student in Chemical Eng., team member
Juliana Ortiz, undergraduate student in Chemical Eng., team member
Olivia Slane, undergraduate student in Chemical Eng., team member

● Faculty/Industry advisors

Hong Yong Sohn, Distinguished Professor in Metallurgical Eng. Dpt., main Faculty Advisor
Michael F. Simpson, Professor in the Materials Science and Eng. Dpt., Faculty Advisor
Zhigang Z. Fang, Professor in the Materials Science and Eng., Industry Advisor

● University and Industry Partners

The University of Utah, Powder Metallurgy Research Lab

● Space Grant Affiliation and Space Grant Director

Utah NASA Space Grant Consortium. Joseph Orr, Director, University of Utah

Table of contents

1. Quad Chart.....	3
2. Executive Summary.....	4
3. Problem Statement and Background.....	5
4. Project Description.....	7
4.1 Description of the Concept.....	7
4.2 Integration of Concept into NASA Lunar Strategy.....	12
4.3 Potential Stakeholders and Funders.....	13
4.4 Technical Specifications.....	13
5. Verification Testing on Earth.....	14
5.1 Reduction of Iron Oxide in Lunar Regolith.....	14
5.2 Carbonylation of Reduced Iron.....	15
5.3 Carbonylation Results.....	16
5.4 Safety Plan and Protocols.....	20
6. Results and Conclusions.....	21
7. Path-To-Flight.....	24
8. Timeline.....	25
9. Budget.....	26
10. Acknowledgements.....	26
11. References.....	27
12. Appendix.....	29
12.1 Appendix A: Real Gas Law, Fugacity, and Equilibrium Conditions.....	29
12.2 Appendix B: Power Consumption.....	30

1. Quad Chart



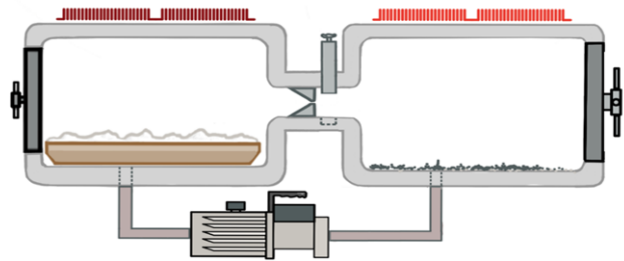
Production of Steel from Lunar Regolith through Carbonyl Iron Refining (CIR)



Concept Synopsis

- In the first stage
 - Metal oxides that were present in the simulant lunar regolith were reduced through CO(g) gas
 - Yields impure iron metal for use in the second stage.
- In the second stage
 - Pressurized CO(g) is used to concentrate the impure iron,
 - obtained from the first stage
 - The product is a high-purity, fine iron powder via the formation and subsequent decomposition of Fe(CO)₅(g).

Image depicting concept



Innovations

- Successful separation and refining of iron from gangue materials via the formation of Fe(CO)₅ (g)
 - With reduced iron powder
 - And with reduced regolith with a low iron content of 6.4wt%
 - At lower temperatures and pressures
- Produced iron powder is immediately usable for additive manufacturing

Verification Testing Results & Conclusions

- Highest reduction was 3.6 wt% Fe after 6 hours under 100% H₂(g) flow
- Highest yield from carbonylation was 45mg at 120°C and 55 atm for approximately 410 minutes
 - Used reduced regolith with 6.4 wt% Fe from Voyager Space
- Verification testing demonstrated compatibility with the systems directly preceding and following CIR
 - Compatibility is demonstrated by magnetically concentrating and subsequently extracting a portion of the reduced iron

2. Executive Summary

Transporting equipment to the moon is extremely cost-prohibitive, and competition is fierce over a limited cargo volume. However, the moon's surface is relatively rich in metal-containing minerals. These factors have motivated the conception of 'Production of Steel from Lunar Regolith through Carbonyl Iron Refining (CIR).' The proposed technology adapts an existing metal production technology on Earth and tailors it into a lunar-optimized two-stage process for separating and concentrating reduced iron in pulverized lunar regolith into a high-purity product, which is subsequently cast or fabricated into useful steel components.

In the first stage, iron oxides in the lunar regolith (up to 22.5 wt%) are reduced to iron. If the iron extraction is a stand-alone operation, a reactive gas such as CO(g) or H₂(g) can be applied to yield reduced iron metal mixed with unwanted gangue minerals. The reactive gas may be produced from CO₂(g) and H₂O(g) found in ice deposits in lunar craters and carbon byproducts from the Sabatier life support system. More preferably, CIR would operate in conjunction with an existing oxygen-producing reduction setup.

The second stage uses pressurized CO(g) to concentrate impure iron into a high-purity, fine iron powder via the formation and subsequent decomposition of Fe(CO)₅(g). Iron carbonyl refining is a commercially proven variation of the well-known Mond process and produces thousands of tons of iron powder annually (Inovar, 2017). The proposed reactor concept optimizes CIR for the lunar environment with a substantially reduced operating pressure and continuous gas cycling to maximize the driving force for Fe(CO)₅(g) formation. A lightened, relatively low-pressure design is a novel direction for a technology that owes economic viability to bulk production in a terrestrial market. However, in a lunar context, the curtailed production is anticipated to be more than compensated by eliminating the high transportation expenses.

The verification testing demonstrated the formation of iron powder in the CIR technology through powder material characterization (SEM-EDS, XRD, particle size distribution, pycnometer). A batch of deoxygenated samples was obtained from the back end of the Pioneer Astronautics process (hydrogen reduction integrated with electrolysis). Compatibility was demonstrated by magnetically concentrating and extracting a portion of the reduced iron. The reduction and carbonylation/decomposition stages may be joined in one single process using CO(g) and under a continuous flow, where further experiments will indicate the kinetics of this process.

Both stages of the CIR had successful experiments. In the first stage, the highest reduction achieved was ~3.6 wt% of Fe after 6 hours under 100% H₂(g) flow. In the second stage, the largest amount of powder was 46 mg from experiment E8, which ran at 120°C and 55 atm for ~410 minutes. Also, reduced powder from the Horizontal Tube Furnace was used to do carbonylation/decomposition experiments, and iron powder was obtained in the decomposition chamber, demonstrating that the two-stage process is feasible starting from simulant lunar regolith. Furthermore, this showed the ability of the CIR system to extract and purify iron and perform with a mineral of low iron content.

The proposed technology is envisioned to support a small, semi-permanent scientific outpost and can be scaled up if desired. It is highly location-flexible and can process crushed lunar rock or common regolith. Iron produced from this method would be printed or cast into steel components, tools, radiation shielding, and structural members. Additive manufacturing offers parts of complex geometry on demand and could become a powerful complement to NASA's philosophy of redundancy. The iron powder produced by CIR is well-suited for additive manufacturing task-specific components, exhibiting an exceptionally small particle size and great sphericity (Bloemacher, 1990). The flow of material from regolith to finished metal requires remarkably little infrastructure in conjunction with additive manufacturing, with the CIR apparatus doubling as a carburization chamber for finished parts. A compact procedure is relevant to the lunar exploration goals in preparation for the 2030s Mars voyage discovery and support of the Artemis mission.

3. Problem Statement and Background

Steel is cemented as humanity's workhorse material on Earth. Natively tough and ductile, the material properties of steel can be manipulated with carbon, alloy additions, and heat treatments to meet demands across a wide range of applications. Despite what steel offers in versatility, it has been a minor component in space missions, largely due to stringent weight limitations on rocket payloads. Improvements in fuel efficiency in recent years notwithstanding, space missions continue to have a cost-per-weight basis on the order of thousands of dollars per kg¹ (Roberts & Kaplan, 2022). With weight at a premium, steel has seen many traditional roles filled by lightweight aluminum and titanium to avoid sacrificing limited payload volume.

The problem of hauling cargo to the moon is circumvented if the required material can be harvested, processed, and shaped at the destination. Iron is an abundant component of lunar regolith owing to a combination of existing lunar geology and millennia of metallic meteor impacts (Badescu 2016). The technical challenge is extracting, concentrating, purifying, and shaping that iron using minimal equipment, without easy access to consumables, and within a hostile environment. Carbonyl iron refining (CIR) offers properties especially conducive to these constraints. With a relatively small amount of equipment, we propose that a lunar habitation using a CIR apparatus can supply its steel components from a common regolith.

The first advantage of CIR in a lunar environment is that the process does not require a regular consumable. The mechanism of formation of iron pentacarbonyl $\text{Fe}(\text{CO})_5(\text{g})$ begins with the reaction (1) of impure iron metal under carbon monoxide to form an iron-bearing gas.



Then, the formation process is thermally reversed in a second chamber by heating the iron pentacarbonyl under a lower pressure to produce a high-purity (>98%) iron powder product through reaction (2).



It can be seen that the carbon monoxide that is absorbed to form the metal carbonyl is released upon disassociation and is immediately available for reuse. Many refining cycles can occur between the replacement of exhausted regolith and the collection of the iron product². The loading/collection process is simple, repetitive, and prime for automation.

A second characteristic of CIR that recommends it for deployment is its affinity for additive manufacturing. The use case for additive manufacturing of lunar iron is compelling. Complex geometry parts can be generated on demand, typically with less than 5% material loss (Ponis 2021). Experimental or habitation components can be printed in advance of the next mission and free up cargo room. Backup components for essential systems can be generated and stockpiled for possible breakages. In an emergency, additive manufacturing could enable engineers on the ground to rapidly design and broadcast one or more CAD files for a custom remedy within hours. In time, this technology could become a powerful complement to NASA's philosophy of redundancy.

Additive manufacturing has great lunar potential but requires a feed powder to meet size and morphology specifications. Exactly what meets the tolerances of particle size varies depending on the additive manufacturing process but is typically in the range of 20-80 μm (M.A. Balbaa 2021, Microtrac 2020). Particles that are large and irregular may introduce defects into the component. They also exhibit suboptimal powder bed density and poor flowability. Most iron production avenues require a post-

¹ For the Saturn 5 launch vehicle, the fuel consumption per unit weight of payload for a lunar mission was roughly 3 times greater than that of an orbital mission (Atkinson, 2020).

² A small amount of carbon monoxide in each batch will react on the surface of the iron via the Boudouard reaction to carburize the metal and form $\text{CO}_2(\text{g})$. The carbon monoxide can be periodically regenerated using unutilized waste methane and/or carbon from the Sabatier life support system (NASA Podcast 2021).

processing step to meet feed stipulations, such as energy-intensive mechanical milling or atomization of the molten metal. In contrast, iron carbonyl powder can be used immediately after being sieved, exhibiting a fine particle size and excellent sphericity (Bloemacher 1990). This final attribute is of particular note, as the reduced packing and flow of irregular particles is aggravated by the moon's reduced gravity and threatens manufacturing complications (Badescu 2016).

Our case envisions a small, semi-permanent scientific outpost that could be scaled up to accommodate a more extensive operation. It is highly location-flexible and can process crushed lunar rock or common regolith. Iron produced from this method would be printed or cast into steel components, tools, radiation shielding, and structural members, considering design constraints arising from iron's ductile-to-brittle transition at low temperatures, such as during lunar nights. The CIR apparatus and reactive gas double in function as a carburization chamber to harden steel components.

The foremost advantages of the iron carbonyl system are its regenerative nature and compatibility with existing life-support systems. Regolith reduction is a fully self-contained process, using hydrogen gas to produce water vapor that is subsequently condensed and separated with electrolysis to provide oxygen for the crew. The ensuing concentration of the reduced iron does not consume a reagent, as the carbon monoxide absorbed to form the metal carbonyl is recovered upon disassociation. What little carbon monoxide is oxidized from batch to batch via the Boudouard reaction can be periodically regenerated.

The primary drawback of iron carbonyl lunar use is the considerable formation pressure. The industry reports pressure values in excess of 200 bar (> 2800 psi) (Inovar 2017). At this pressure, the vessel wall thickness would be substantial and make the vessel extremely heavy. We propose experimenting with formation pressures of 60 bar or less with a proportional decrease in formation temperature to counteract the shift in system equilibrium. Although slower kinetics are anticipated with these changes, it is reasonable to assume that a lunar base will not require iron at the same commercial throughput rate that the earth-bound industry is beholden to remaining profitable.

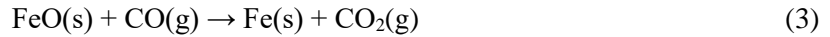
An additional challenge is that iron carbonyl formation is exothermic and will drive the equilibrium out of favorability if a balance between heating and cooling is not maintained, a situation complicated by the lunar environment. In this paper, several heating and cooling aspects of the design have been examined.

A final concern is the possibility that a proportion of the iron pentacarbonyl will decompose on reactor surfaces and adhere strongly rather than forming a usable particle product. This issue was not observed in our experiments but could present challenges in some designs.

4. Project Description

4.1 Description of the Concept

Iron is present in lunar simulants such as Pyroxene (FeSiO_3), Olivine (Fe_2SiO_4), Glass-Rich Basalt (Fe_2O_3 , Fe_3O_4 , FeO), and Ilmenite (FeTiO_3). Among the Apollo and Luna mission samples, the iron oxide concentration in the lunar regolith ranged between 0.7 to 22.5 wt%, with an average value of 14.8 wt% (Badescu 2016). However, before carbonylation can concentrate and purify the iron, it must first be reduced to its elemental form. Our group originally envisioned a CIR concept that performed its own regolith reduction followed by CIR extraction, both stages using reactive carbon monoxide gas. The reduction reaction of the various iron-bearing compounds can be generalized as follows,



It is feasible that a CIR apparatus could work as a stand-alone process at the sacrifice of requiring far more frequent regeneration of the CO(g) from $\text{CO}_2\text{(g)}$. However, operating in isolation is probably unnecessary because of the considerable attention and resources the space community has invested in technologies to extract oxygen from lunar metal oxides. When one considers that ~90% of a rocket's initial weight is rocket fuel and typically 70-80% of that fuel weight is liquid oxygen (LOX), sourcing the oxygen for the return trip at the destination promises enormous dividends³ (NASA-A, 2021; Aerospace America, 2021). Approaches to reducing the metal oxides are diverse and are not limited to hydrogen reduction, molten salt electrolysis, and carbothermal reduction. A carbonyl reactor is envisioned to play an unobtrusive supporting role in an existing reduction setup by processing the deoxygenated regolith. When CIR operates in this role, the equipment volume required to go from raw regolith to finished metal components is remarkably compact, as shown in Figure 1.

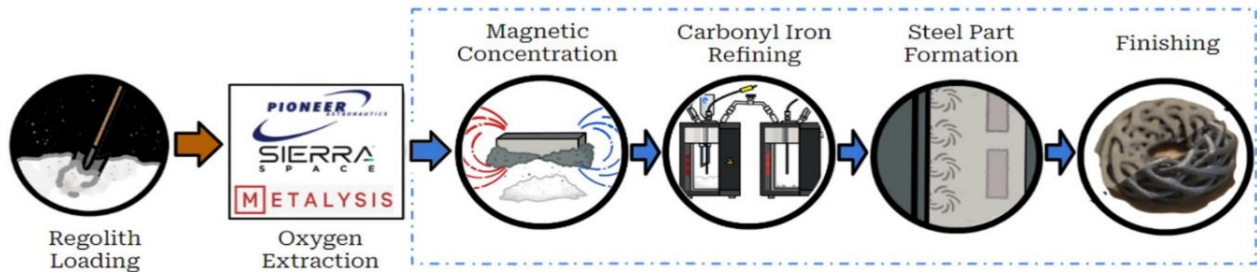


Figure 1: Proposed concept of the CIR iron production technology.

Assuming that oxygen extraction will operate at a scale required to supply fuel demands, a modest-sized CIR apparatus would have a smaller throughput and benefit in efficiency by magnetically concentrating the larger quantity of reduced regolith. This mitigates the impact of being in a location with an initially iron-poor feed. The feed can be additionally supplemented with iron nanoparticle powder magnetically collected on a stroll across the moon's surface. Solar winds may have reduced as much as 10% of iron to metallic form and iron nanoparticles from meteor impacts (Korotev 2023). The magnetic collection of iron from unprocessed lunar dust has experimental precedent (NASA, 2006). Suppose mobile magnetic collection is proven successful in practice. In that case, it seems reasonable that carbonyl concentration would be uniquely capable of processing such a feedstock and might not require a prior reduction step. For this project, it was assumed that carbonylation is acting in tandem with a reduction technology and assumes a reduction throughput that allows for magnetic concentration.

³A means of $\text{O}_2\text{(g)}$ generation is also essential for long-term habitation to offset the minor but unremitting losses experienced by reprocessing systems. Reducing 120 kg of Ilmenite with $\text{H}_2\text{(g)}$ can produce 1.5 kg of water daily to meet one astronaut's needs (Badescu 2016).

Commercial Carbonyl Iron Refining (CIR) Production

The commercial application of carbonyl iron refining was first envisioned in the 1920s and pioneered by BASF, producing around 29,000 metric tons per year of iron powder (Inovar 2017). A visual summary of the carbonyl iron refining process used by BASF is shown in Figure 2. Carbonylation begins by reacting unrefined iron granules (or sponge iron) under pressurized $\text{CO}(\text{g})$ to form $\text{Fe}(\text{CO})_5(\text{g})$. The reaction favors the $\text{Fe}(\text{CO})_5(\text{g})$ formation product at low temperatures. However, the reaction is kinetically limited and extremely sluggish at low temperatures. Commercially, the compromise between kinetic and thermodynamic factors is found in the range of 150 to 200 °C. To maximize yield, the formation pressure is reported to be greater than 200 atm (Inovar 2017, Bloemacher 1990). These conditions are held for 120 hours and achieve ~65% extraction of the iron. The chemistry closely parallels the Mond process used for refining nickel. If both nickel and iron are present in the initial sample, a mixture of both metal carbonyls will be in the gas phase. A distillation step separates the metal carbonyls based on boiling point. Depending on the decomposition conditions, the iron product will range in size from microns to centimeters in diameter. Iron is ~97% pure, with less than 1 wt% of carbon (Inovar 2017).

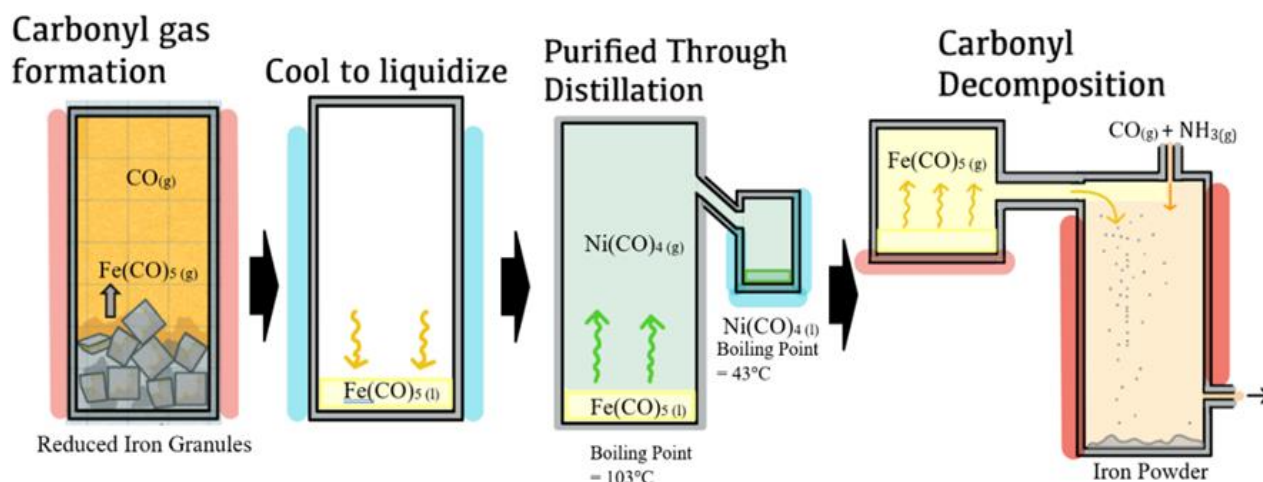


Figure 2: Simplified scheme of commercial carbonyl iron refining. Adapted from Inovar, 2017; Bloemacher, 1990. This flow is treated as a flow representation only, as images of the steps and equipment could not be located.

The Feasibility of Low-Pressure Carbonyl Iron Refining (CIR)

Little discussion could be found in the literature on applying carbonyl iron refining to a lunar environment. This may be partially a result of its relative obscurity against the backdrop of a massive global iron industry on Earth. Carbonyl refining produces a minuscule fraction of the annual steel tonnage and only from a single facility. More likely, researchers considering the process may have dismissed it on account of the >200 bar formation pressure used by BASF.

Operating at high pressure, especially in an environment that complicates inspection, raises concerns about safety and the excessive weight of robust components and thick vessel walls. These relevant reservations represent the primary challenge to off-Earth iron carbonyl refining. HSC Software (Roine, 2002) was used to determine the thermodynamic feasibility of the reactions within optimal temperature and pressure ranges and suggest appreciable $\text{Fe}(\text{CO})_5(\text{g})$ formation at pressures as low as 30 bar.

Little literature could be found exploring CIR at lower pressures, where a compensatory reduction in temperature would produce the iron at a rate too slow to remain commercially competitive in the global market. However, low-pressure and low-temperature conditions appear ideal for extraterrestrial environments, where curtailed production would be more than compensated by eliminating transportation expenses. Two studies support the viability of low-pressure formation. A 2013 laboratory study demonstrated the extraction of Fe and Ni from reduced ore using the carbonyl process at only 60 bar and

180°C with a good iron yield (>70%) in excess of 1 kg and excellent kinetics (≥ 48 hours) (Terekhov & Emmanuel, 2013). A 2015 thesis that we located after our mid-project studied $\text{Fe}(\text{CO})_5(\text{g})$ formation at very low temperatures (80-100°C) under continuous, 54 atm $\text{CO}(\text{g})$ flow and recorded formation rates of 0.45-0.75 wt% Fe carbonylation/h (1 g original mass) (Cui, 2015). These moderate formation kinetics, previously considered too low for practical kinetics, inspired us to decrease our temperature floor from 150 to 120 °C.

Analysis of the literature leads to the hypothesis that operating the CIR process at a reduced pressure on the order of 50-100 atm will generate a sufficient iron throughput to exceed the reactor weight and produce a useful excess in a reasonable operating time. The validity of this hypothesis requires verifying that reaction kinetics are sufficiently rapid, as discussed in Section 5.

Proposed Carbonyl Iron Refining (CIR) Two-Chamber Design

This research project adapts the existing metal production technology and tailors it into a lunar-optimized two-stage process, referred to in this paper as the CIR apparatus. Reduced lunar regolith is loaded into the formation chamber and is subjected to a high $\text{CO}(\text{g})$ partial pressure, maintained at an appropriate temperature to maximize iron carbonyl formation (Figure 3A). A small but continuous gas flow is allowed to pass into the lower-pressure decomposition chamber, where a higher temperature and lower pressure favor iron powder formation (Figure 3B). A high-power compressor operates at regular intervals to maintain the pressure difference between the two chambers.

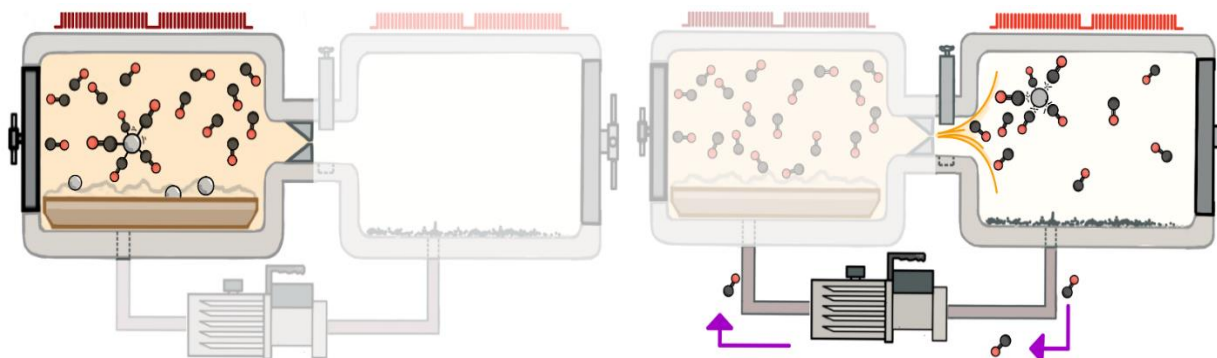


Figure 3: Concept Design for a lunar Carbonyl Iron Refining (CIR) apparatus: A) Production of iron pentacarbonyl in the formation chamber; B) Iron powder generation in the decomposition chamber

The iron product is periodically collected by sealing the center aperture, maintaining the compressor, and finishing with a vacuum pump and small bleed tank (not pictured). Exhausted regolith is switched out periodically by reversing the direction of the pump again assisted on the final stretch with the vacuum and bleed tank.

Distillation is absent in the CIR aperture. Certain metal impurities with $\text{CO}(\text{g})$ affinity, such as Ni and Co, have a relatively small abundance in the lunar regolith. These components could appear in small amounts in the iron product, especially nickel. This is not anticipated to be an issue. If a separation between nickel and iron is imperative, then distillation can be accomplished in the apparatus by cooling the formation chamber to between 43 °C and 103 °C to isolate $\text{Ni}(\text{CO})_4(\text{g})$. The CIR apparatus could theoretically harvest high-purity nickel powder by tracing surface magnetic anomalies to Fe-Ni meteor impact craters (Ellery, 2020).

Titanium is the material for the vessel walls because the carbonyl process may pit or otherwise weaken steel or nickel inner surfaces. Additionally, an embrittled steel reactor could rupture in the cold of the lunar night cycle if power is lost to the heating system for an extended period. Titanium components have an excellent strength-to-weight ratio and will reach the break-even point of producing an equivalent weight in iron product more quickly. Both heating and cooling systems will be required for operation, as the formation process is exothermic and will require active heat removal if the reaction kinetics are sufficiently fast. Energy consumption projections will be visited in greater detail later in this section.

Loss of Power Safety Assessment

The consequences of a sudden loss of power have been considered. The four powered systems are the heating elements, cooling elements, compressor, and the vacuum pump. If the loss of power occurred during regular operation, the immediate effects would be the gradual heating of the formation chamber (inactive coolant circulation), gradual cooling of the decomposition chamber (inactive heating elements), and the equalization of pressure between the two chambers (inactive compressor). None of these effects pose a danger to personnel or equipment. The formation chamber would initially rise in temperature due to the heat from the exothermic reaction. Due to sluggish formation kinetics, the corresponding decrease in $\text{Fe}(\text{CO})_5(\text{g})$ equilibrium pressure at the higher temperature and lower pressure will keep the heating in check as a new equilibrium is established, with near certainty well under the 300°C allowed peak temperature. A mirroring state of conditions will develop in the decomposition chamber as the pressure equalizes between the chambers and conditions swing toward very slow $\text{Fe}(\text{CO})_5(\text{g})$ formation. If the power is off for an extended period and temperatures drop below 103°C , the $\text{Fe}(\text{CO})_5(\text{g})$ will condense into a liquid phase. This is not anticipated to be problematic and will revert when the heating is restored.

Predicting Equilibrium Conditions in a Physical System

Although HSC initially established thermodynamic feasibility, it was decided that a more comprehensive program would be needed to inform experimental decision-making. A predictive model was created in Python that tailored equilibrium quantities to the physical parameters of the carbonylation and decomposition of carbonyl iron experiments. The inputs to the model made it flexible regarding the total volume of the chamber, the experimental conditions of operating temperature and the initial partial pressure of $\text{CO}(\text{g})$, and the characteristics of the lunar regolith as the total mass, weight percent iron, tap density, and true density. Thermodynamic values of ΔH and ΔS for the formation of $\text{Fe}(\text{CO})_5(\text{g})$ were extracted from HSC Software, which allowed for the calculation of the standard free energy of formation ΔG° as a function of temperature. The equilibrium conditions are calculated iteratively by adding to the system a small quantity of ζ moles $\text{Fe}(\text{CO})_5(\text{g})$ while subtracting ζ moles of $\text{Fe}(\text{s})$ and 5ζ moles of $\text{CO}(\text{g})$. The pressure and volume are adjusted accordingly until the equilibrium is satisfied. Solid volume contraction and gas volume increase are accounted for as solid iron enters the gas phase. This factor is of modest importance for single pressurizations. Still, it increases in relevance when multiple rounds of extraction are performed on the same batch, especially at moderate to high iron concentrations. The model derivation is found in Appendix A.

Figure 4 shows the predictive model applied to the formation chamber we utilized in verification testing, to be formally introduced in Section 5. Linking the equilibrium concentrations to the dimensions of the reactor vessel allows for projections to be made concerning the number of complete formation cycles to be completed before the CIR apparatus breaks even and produces a greater mass than its weight. Figure 4B gives an additional helpful insight. When initial $\text{CO}(\text{g})$ partial pressure is varied while temperature and regolith characteristics are held constant, an increasing difference is observed between the initial pressure and the equilibrium pressure. This pressure drop occurs because 5 moles of $\text{CO}(\text{g})$ are consumed for every 1 mole of $\text{Fe}(\text{CO})_5(\text{g})$ generated from reaction (2), for a net loss of 4 moles. This pressure drop provides a way of roughly estimating the reaction progress by regularly recording pressure values. Figure 4B shows that this method of monitoring the reaction rate becomes infeasible at low $\text{Fe}(\text{CO})_5(\text{g})$ equilibrium partial pressure, where pressure changes are too small to be detected or can be confused with pressure fluctuations caused by changes in temperature.

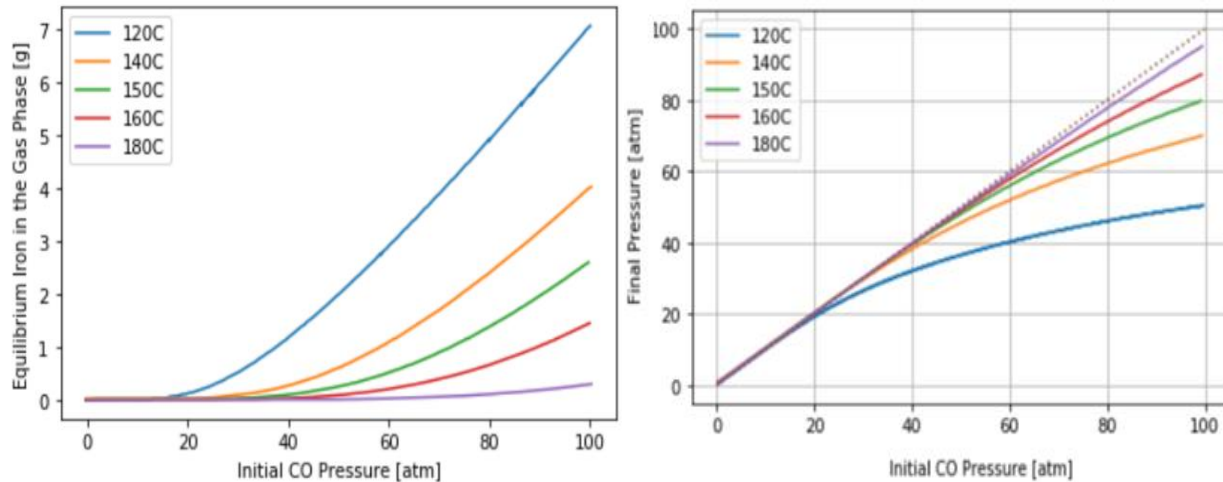


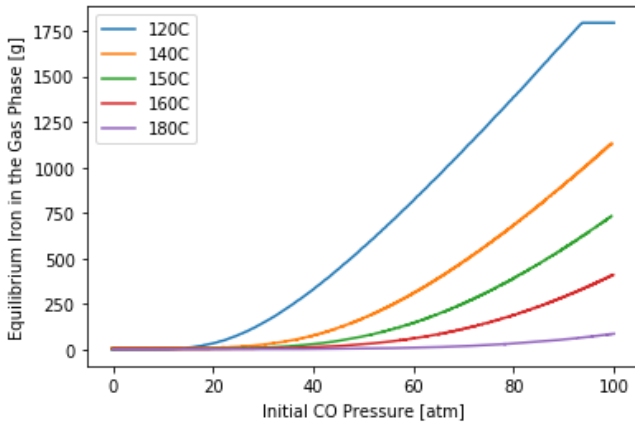
Figure 4: A) Iron equilibrium yield between 120-180 °C in the gas phase. The physical and experimental parameters are a chamber volume of 0.4 liters, 10% solids loading, and 10wt% Fe with 59.6% porosity. B) Initial CO(g) pressure vs final system pressure.

Break Even Yield

For the purposes of predicting yield the CIR apparatus as a scaled-up version of our 0.6-liter laboratory scale titanium formation chamber. The CIR apparatus is envisioned as two similarly proportioned 100 L chambers connected end-to-end. Each cylinder has a length of 1.092 meters with a 0.341-meter diameter. Scaling up the weight of the 1.6 kg laboratory-size formation chamber predicts a 249 kg mass. This mass appears to be excessive of demands. For example, two steel K cylinders weigh a combined 120kg, have a combined 100 liters of volume, and can easily withstand 100atm. Therefore, we will instead use the mass of two K-cylinders multiplied by the Ti:Fe density ratio for a conservative estimate of 70 kg. Combining the mass of the formation and decomposition chambers totals 140kg. The mass of the compressor, finishing vacuum pump, heating and cooling elements, and small bleed tank are estimated as an additional 25% of the apparatus mass for 210 kg total.

Projections for equilibrium iron yield in the gas phase can be seen in Figure 5 to range from 1750 g at 120 °C to 80 g at 180 °C. Other than volume, the loading characteristics are the same as used in Figure 4. At 120 °C, the gas phase can accommodate more iron in $\text{Fe}(\text{CO})_5(\text{g})$ than in the 10 liters of solids, causing the yield to plateau. At other temperatures, the regolith could be pressurized multiple times, if desired, to extract additional iron before the exhausted regolith needs to be switched out. Low temperatures are seen to be thermodynamically favorable. Still, it should be recalled that the kinetic limitations at lower temperatures mean that many high-temperature equilibrium cycles could likely be completed before a lower-temperature equilibrium is reached, necessitating verification testing to clarify what temperature/pressure combination gives the best yield.

Table I chooses the 150 °C isotherm and examines the number of cycles required to produce a mass of iron powder equal to 210kg. The data reinforces the rationale for industry to opt for high formation pressures in commercial production. If the equilibrium code can be experimentally verified, it is hoped that cycles to break even will be useful for advising reaction conditions.



Pressure [atm]	Iron Mass per Cycle [g]	Cycles to Break Even
20	3.7	56,757
40	29	7,241
50	72	2,917
60	145	1,448
80	389	540
100	732	287

Figure 5: A) Iron equilibrium yield between 120-180 °C in the gas phase. The physical and experimental parameters are a chamber; B) Equilibrium cycles required to produce the mass of the CIR apparatus at 150 °C.

Estimated Energy Consumption

One of the first aspects of CIR that stands out when listed alongside competing concepts is the relatively low maximum operating temperature of 300 °C. It is tempting to flaunt energy conservation as a primary selling point for the concept, but low operating temperature must be weighed against slow formation kinetics. A modest size CIR apparatus must continually operate to meet iron quotas.

The primary areas of energy consumption are: 1. Replacing heat lost to the environment; 2. Continual or intermittent compressor operation to maintain the pressure gradient; 3. Heating the gas entering the decomposition chamber; 4. Cooling the gas entering the formation chamber. Table I gives very rough estimates for power consumption for the CIR apparatus of previously described dimensions with 180°C and 80 atm in the formation chamber and 300°C and 60°C in the decomposition chamber. The equations used to produce these values are located in Appendix B.

Table I: CIR estimated power consumption at lunar temperature extremes

Scenario	Temperature [K]	CIR Estimated Power Consumption [W]
Polar night	50	5284
Equator night	95	3748
Polar day	200	4822
Equator day	397	1665

4.2 Integration of Concept into NASA Lunar Strategy

The NASA Artemis missions are an exploration, study, and sustainable development of the lunar surface using permanent human-robotic presence, with the consequent mission of sending the first astronauts to Mars. Since there is a high cost of transporting raw materials from Earth to the Moon, infrastructure construction for a lunar base using in-situ resources is critical to validate technical operations (Loff & Dunbar, 2019). A strategic and sustainable presence on the lunar South Pole will be established after successfully landing on the Moon. The diverse activities on this Artemis Base Camp will contribute to the spaceflight development of the production research projects and demonstrate elements of a Mars-forward architecture in American space leadership. Also, the Volatiles Investigating Polar Exploration Rover (VIPER) data will allow for future In-Situ Resource Utilization (ISRU) technologies. Rovers will be used to obtain detailed information on the availability and extraction of usable resources such as water and

oxygen. These resources may be used as long-term supplies for the production technology implementation on the Moon to decrease the supply needs from Earth (NASA-A, 2021).

The proposed innovative technology of producing iron powder starting from iron oxide present in lunar regolith through the formation and subsequent decomposition of iron-carbonyl has the potential impact on creating final steel products in a cost-effective operation through an innovative technology, which may thrust the private industry and international partners towards the preparation of the 2030s Mars voyage discovery and exploration to support the Artemis mission. The possibility of generating new or backup pieces for the equipment through 3D printing allows for a permanent presence on the lunar surface. The system's potential for mobility and ability to operate under extreme temperature conditions during cold/day cycles can contribute to using this technology in different sections of the Moon, whose resources are dispersed and whose geography is complex.

4.3 Potential Stakeholders and Funders

CIR technology has an impactful potential for various stakeholders and funders to develop 3D printing of steel with the produced iron powder. A possible funder is Pioneer Astronautics, a research and development company dedicated to new space technologies. The company has provided samples of reduced lunar regolith simulant (similar to NASA JSC-1a) through hydrogen and integrated with electrolysis, with various amounts of metallic iron for the development of the carbonylation and decomposition of carbonyl iron formation testing. Their R&D as an industry would be of interest for testing reduced samples and implementing the CIR technology with an automated system on a bigger scale. The company intends to develop the production of oxygen and steel from lunar raw materials to continue with its Moon to Mars Oxygen and Steel Technology program. Energy savings could be attained by avoiding thermal energy related to non-metallic constituents' heating and phase changes. Therefore, substituting carbonyl refining for the melt refining unit operation the company uses could significantly advance their technology.

4.4 Technical Specifications

While identifying the optimal formation temperature and pressure for acceptable kinetics is the key to confirming feasibility, a secondary aspect that warrants study is to devise a means to control iron deposition. The equilibrium shifts dramatically toward decomposition in the decomposition chamber when $\text{Fe}(\text{CO})_5(\text{g})$ is heated past 200 °C. In contrast to $\text{Fe}(\text{CO})_5(\text{g})$ formation, the decomposition step is rapid. Fine spherical iron crystal nuclei form in the heated zones and exhibit hailstone-like growth layers along their descent to the chamber bottom (Bloemacher, 1990). Literature implies that nucleation is homogeneous. Heterogeneous nucleation, which is kinetically favorable over homogeneous nucleation, could present a challenge in a small chamber. Iron nucleated on an existing surface will not take on a powder morphology and may strongly adhere to said surface. This possibility is doubly problematic, representing both an effective loss of iron product and a gradual constriction of the formation chamber. Care must be taken to delay contact between the loaded gas and the chamber walls for as long as possible.

The NASA Technology Readiness Level (TRL) assesses the maturity level of the technology (NASA, 2020). The overall TRL predicted is 6.55, whose contributions are detailed as follows: $\text{Fe}(\text{CO})_5$ production has been established in the industry for over 100 years, for which a TRL of 8 (ground demonstrated) is assigned, and approximately 60% of the proposed system uses this technology; Pumping and vacuum systems are well understood on Earth, but the lunar environment complicates their application. A TRL of 4 is assigned and weighs 30% of the system complexity; Heating systems are better understood, with a TRL of 6, and weigh 5%; Cooling systems have a TRL of 5 with 5% weight. A reliable engineering unit that addresses all critical scaling issues was built and demonstrated in an appropriate simulated operational environment.

5. Verification Testing on Earth

5.1 Reduction of Iron Oxide in Lunar Regolith

A laboratory setup analogous to the CIR apparatus was designed, constructed, and implemented to test the proposed novel two-step carbonyl iron refining (CIR) application. In the first project stage, metal oxides in the simulant lunar regolith were reduced through CO(g) reducing gas to yield iron metal for use in the second stage. The Lunar Mare (LMS-1) High-Fidelity Moon Dirt Simulant from Exolith Labs was chosen for its compositional and particle size similarities to the Lunar Mare regions on the Moon. According to XRF, 8.6 wt.% FeO is held within iron oxides and iron silicates (Exolith Lab, 2023). The anticipated iron concentration is calculated to be approximately 2.1 – 6.7 wt.% Fe.

In the reduction stage, the lunar regolith simulant is loaded onto ceramic trays in a sealed Horizontal Tube Furnace (HTF) built at the University of Utah's campus. The HTF from the MTI Corporation system is shown in Figure 6, which uses CO(g) at ambient pressure and is flushed before and after experiments with N₂(g). Reduction takes place at high temperature (~1000 °C) with CO(g), and the gas lines are controlled through pressure regulators and flowmeters, and the off-gas flows from a bubbler to the fume hood, where residual CO(g) is burned using a Bunsen Burner. Also, surface-mount and personal CO(g) detectors are always used during operation, and the system is constantly monitored for leaks. MoSi₂ heating elements heat the stainless-steel reaction tube, and it is water-cooled on both ends. An internal thermocouple indicates the reaction temperature in the isothermal zone, and Kaowool is an insulator on the reaction tube.

The design of experiments in the HTF considered temperature, residence time, and gas partial pressure variables. The temperature decided upon was 1000 °C. The residence time was planned at 10 minutes, 30 minutes, 1 hour, and 3 hours. The lunar regolith powders (mean particle size 91 μm) were dried at 200°C for 24 hours before each experiment, where a 0.32 wt% loss on average was observed. The mass loss is expected due to water vaporization and not an off-gas, given the relatively low drying temperature. An oxidizing procedure was also developed where samples were held at 1000 °C for 24 hours. Four different methods were selected in the reduction experiments as possible procedures for obtaining reduced iron from lunar regolith: dried lunar regolith (LR), dried lunar regolith mixed with carbon powder (LRC), oxidized lunar regolith (OLR), and oxidized lunar regolith mixed with carbon powder (OLRC).

As a product of an experiment, a portion of each powder reduced was analyzed to determine iron concentration and extent of reduction. Initially, the reduction stage was of considerable importance, as some form of reduced regolith simulant would be required. Shortly after the mid-project report, Pioneer Astronautics generously sent 4 kg of their beneficiated regolith simulant, largely eliminating the need to reduce our regolith. One carbonylation (E11) was performed on our in-house reduced sample.

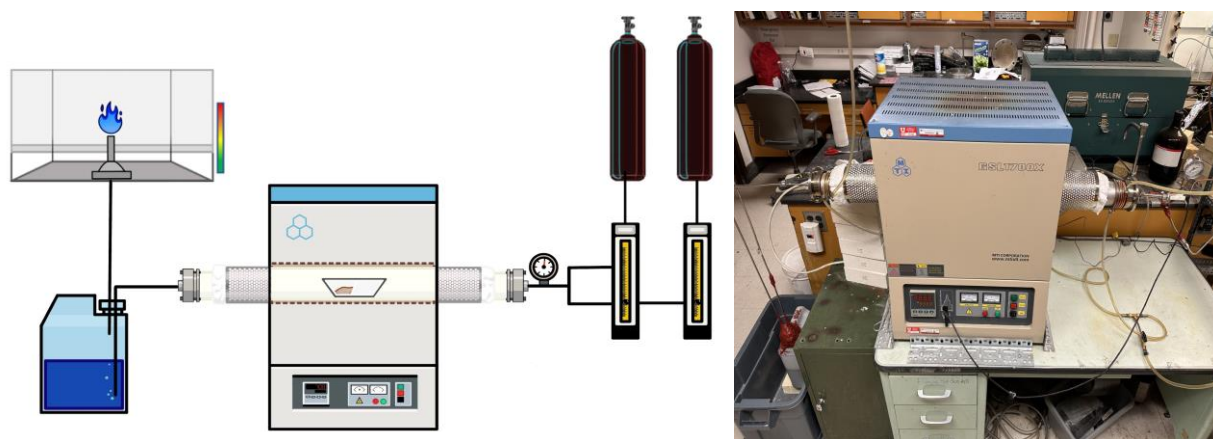


Figure 6: First stage of iron oxide reduction in a Horizontal Tube Furnace:
A) System and subsystems diagram; B) Laboratory setup

Quantifying the Extent of Iron Reduction

A challenge was faced regarding accurate iron quantification because of several constituents present in the reduced lunar regolith. To mitigate it, Pioneer Astronautics (PA, now Voyager Space) was contacted regarding their quantification method of metallic iron. The company used the inductance variable of a copper coil to determine the iron content in a powder sample. An inductance setup (Figure 7) was assembled and tested based on the concept from Pioneer Astronautics, which included a 3D-printed receptacle to hold a powder sample container, a copper coil, glass vials, and an LCR Meter. The setup was calibrated with various 4-gram standards, each containing a specific weight percent of iron offset with silica. Approximately 4 grams were prepared and placed into the 3D-printed receptacle to measure the iron content of a sample. The change in the inductance value was recorded and plugged into the calibration curve to calculate the iron content.

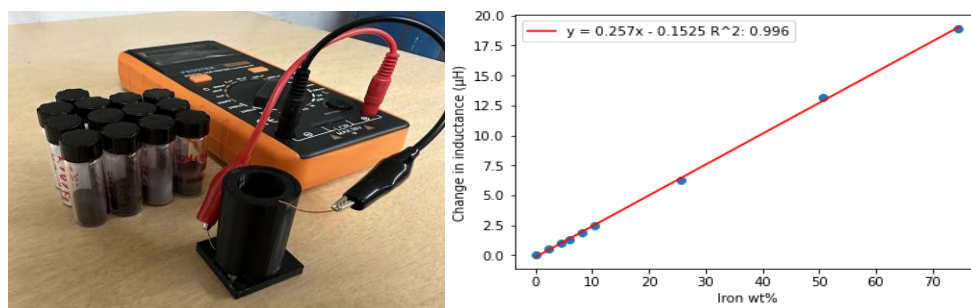


Figure 7: Induction method: A) Laboratory setup; B) Calibration curve.

The inductance of a coil is directly proportional to the magnetic permeability of its core sample. As the amount of iron in the core material increases, the coil's measured inductance also increases, indirectly allowing the iron content measurement. All constituents within the lunar regolith simulant were tested to ensure an accurate measurement of the iron content, and none significantly affected the inductance. Iron quantification was accomplished in the reduction experiments using this induction method, and concentrated materials were also checked into the second stage carbonylation. The highest reduction achieved was ~3.6 wt% of Fe after 6 hours under 100% $H_2(g)$ flow. This number may be due to the limited amount of Ilmenite in the lunar regolith sample along with the difficulty of Olivine and Pyroxene reduction. In the exploration of lunar regolith reduction samples, pure Olivine was reduced, experiencing a maximum metallic iron content of 2.15 wt%, and pure Pyroxene was reduced, experiencing a maximum of 1.37 wt%. The limited amount of metallic iron produced from Olivine and Pyroxene is a contributing factor to the total limited amount of iron in the reduced regolith, as they are major components in the lunar regolith simulant. The limited ability of Olivine and Pyroxene to be reduced is probably due to the formation of silica shells and layers.

5.2 Carbonylation of Reduced Iron

In the second project stage, a scaled-down version of the two-chamber design was tested for the thermodynamics and kinetics of $Fe(CO)_5(g)$ formation and decomposition stage to obtain $Fe(s)$ powder. The reduced lunar regolith was loaded into a system composed of one 0.6-liter titanium pressure vessel from Parr Instruments and a 19-liter stainless steel pressure vessel, which is sheathed in a removable aluminum layer and heterogeneous nucleation will not damage the equipment or prevent the determination of the iron yield mass. As shown in Figure 8, the apparatus is located inside a fume hood to safely vent away $CO(g)$ in the case of a leak.

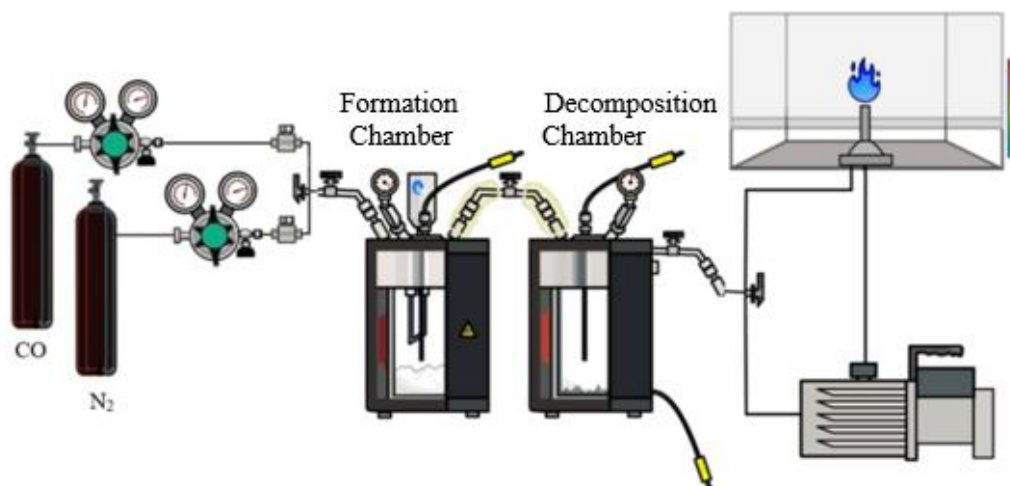
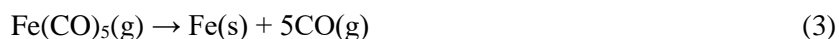


Figure 8: Laboratory setup of the second stage of carbonyl iron formation and decomposition

The Fe(s) present in the lunar regolith sample is separated through the carbonyl iron gas formation given in reaction (2), which will be transferred as a gas phase into the second pressure vessel, for its subsequent decomposition to purified Fe(s) through reaction (3).



The system was vacuumed, and the first vessel was pressurized with CO(g) and brought to carbonyl iron formation temperature. Temperature and pressure combinations were tested to find optimal kinetics of carbonyl iron formation, with a pressure maximum of 55 atm and a temperature minimum of 120 °C. Water tubes act as cooling elements when the formation is initiated, and heat begins to be produced. Once the Fe(CO)₅(g) has been monitored throughout the pressure variation in the pressure gauge, and once its formation has been accomplished, the decomposition should be favored in the second vessel by increasing the temperature to 200 °C and decreasing the pressure to 5 atm so that iron is deposited on the bottom part of the chamber. The system is depressurized by opening one of the exit valves, and the system is flushed with N₂(g) to ensure there is no CO(g) or carbonyl iron left inside the system. If results indicate a relatively small powder proportion, the decomposition chamber temperature may be increased from 200 °C to as high as 300 °C. In a mature design, automated elements of pressure gauge reading are anticipated to assist with operation. The loss of power during the use of the vacuum pump is unlikely due to its infrequent use before the new lunar regolith is loaded into the system. No adverse consequence is anticipated, as all but a small amount of CO(g) will be independently contained in the decomposition chamber that will be burnt in the off-gas.

5.3 Carbonylation Results

In the testing of the CIR system for prospective lunar regolith deployment, eleven carbonylation/decomposition experiments were performed. Each experiment explored a range of temperatures (120 - 150 °C), pressure (50 - 55 atm), and input load material (synthetic Iron Puriss powder Aldrich 12310 of purity ≥ 99%, lunar regolith from Pioneer Astronautics containing 3.2 - 13.8 wt% Fe, lunar regolith obtained from Horizontal Tube Furnace), which are detailed for each experiment in Table II.

Table II: Summary of Carbonylation Experiments.

Experiment	E1	E2	E3	E4	E5	E6	E7	E8	E9	E10	E11
Configuration	Batch	Continuous	Batch	Batch	Batch	Batch	Batch	Batch	Batch	Non-Cooled Batch	Batch
Input load material	Synthetic Iron Powder	Synthetic Iron Powder	Synthetic Iron Powder	Synthetic Iron Powder	Lunar Regolith PA	Synthetic Iron Powder	Synthetic Iron Powder	Lunar Regolith PA	Lunar Regolith PA	Lunar Regolith PA	Lunar Regolith HTF
Pressure (atm)	50	50	55	55	55	55	55	55	55	50	55
Temperature (°C)	150	150	120	150	150	130	140	120	120	150	120

All batch experiments involved preloading the reaction vessel with synthetic pure iron or lunar regolith powder from Pioneer Astronautics or Horizontal Tube Furnace and CO(g) to a determined total pressure. After loading, the reaction vessel was heated to the targeted temperature and pressure. The CO(g) load pressure was precalculated to achieve the desired experimental pressure after heating. Some fluctuation within the starting pressures is due to experimental error, as hand loading with an analog pressure gauge may be imprecise. The experiment E2, a continuous flow experiment, involved the same loading step as batch processing, but after experimental temperature and pressure were reached, needle valves in the system were opened and adjusted as needed to maintain pressures in all chambers. The flow rate in this experiment was unknown and generated a lack of flow control, which discontinued continuous flow experiments in this project. The continuous configuration could be tested by installing a flow controller in the system. The last type of experiment conducted was a non-cooled batch. This experiment had the same conditions as a regular batch process experiment, except external cooling was turned off. This was done to confirm the expected behavior present in a carbonylation reaction.

In the experiments, E3, E5, E6, E7, E8, E9, and E11 all produced product powder collected in the decomposition chamber. During some of these experiments, the iron powder had ceramic and rubber materials from the testing apparatus, which were easily removed. The recovery of iron powder for these experiments is shown in Figure 9. The largest amount of powder recovered was in experiment E8, which ran at 120 °C and 55 atm for ~410 minutes. The powder loaded for this experiment consisted of reduced lunar regolith from Pioneer Astronautics with ~6.4 wt% Fe. On the other hand, experiment E11, which ran at similar conditions to experiment E8, considered the loading of reduced simulant lunar regolith from the HTF with ~1.37 wt% Fe. Iron powder product was collected in both experiments, demonstrating the ability of the CIR system to extract and purify iron from a starting material. It showed the ability of the system to do so with lower iron content, as most theoretical calculations were run with 10 wt% Fe.

During each experiment, the carbonylation chamber temperature and pressure were logged at consistent intervals to track changes and general trends. Using Experiment E8 as a reference for the batch process, a pattern was common among the experiments. Between the start of the experiment and the first data point, most batch experiments showed a temperature spike of between 3 and 10 °C, as shown in Figure 9. Possible explanations for this spike are PID overshooting, the system's difficulty reaching thermal equilibrium, and the high initial reaction rate. By the first data point, the carbonylation chamber had reached equilibrium and held a steady temperature with few fluctuations.

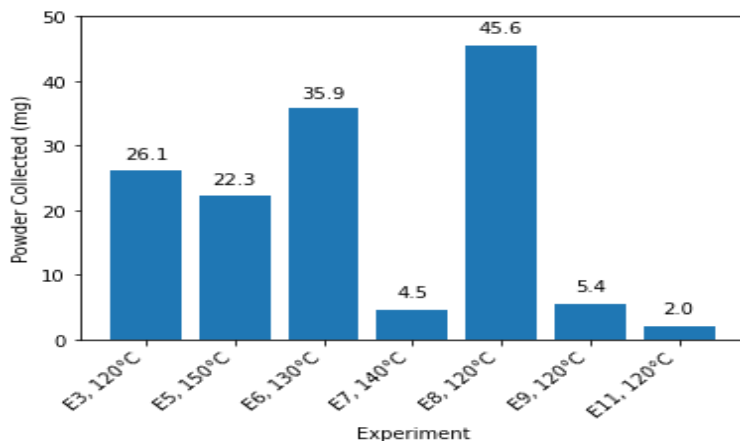


Figure 9: Iron powder collected from the decomposition chamber in carbonylation experiments.

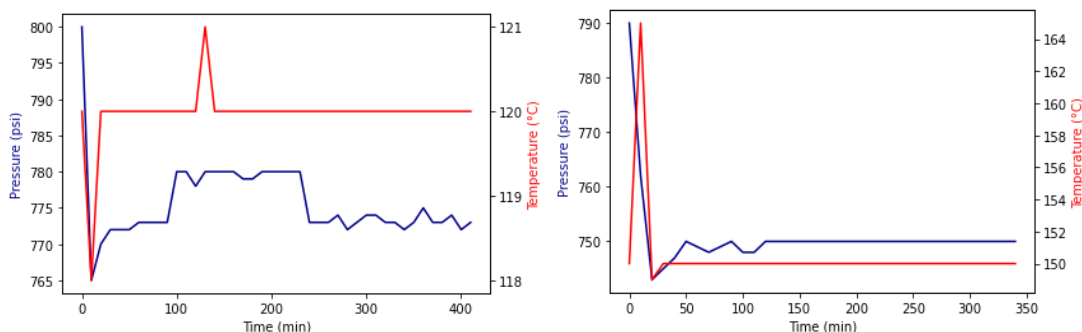


Figure 10: Pressure and temperature versus time for experiment A) E8 (cooled batch process); B) E10 (non-cooled batch process).

The pressure had much larger fluctuations than temperature. The largest change to pressure for E8, as seen above, and the other experiments occurred within the first half hour to 45 minutes. After slowly increasing in pressure during the heating stage, the carbonylation chamber would hold at a peak pressure momentarily and then experience a rapid decrease of between 25 and 40 psi, as shown in Figure 10. The drastic change and the consistency with which this occurred may indicate a very fast initial reaction rate or a rapid cooling of the gas after the thermocouple reaches temperature. The pressure would generally stabilize with fluctuations of ± 10 psi for the rest of the experiments. Some experiments would show a downward trend in the pressure after the initial decrease, but this was not consistent and was challenging to decipher with the noise in the data.

Three tests were conducted to increase confidence in the experimental results of the system: dry heating, rapid pressure release, and batch process without cooling. The dry heating test was done to see if the fluctuations seen in the experiments were due to the experimental apparatus or chemical reactions. During this dry heating, no major fluctuations were apparent, and any present were in the magnitude of 2 psi, not the ± 10 psi seen in experimentation. One possible explanation for pressure fluctuations during the experiment is the water-cooling pipe running inside the formation chamber. Iron pentacarbonyl in this setup may be condensing on the cooling pipe and building up droplets that then fall onto the charge and rapidly evaporate in a cyclical nature. Other explanations could be the increased sensitivity of the pressure gauge at high temperatures and pressures to jostling or vibrations.

The rapid pressure release test of the experiment through CO(g) and an inert powder was performed. The system was heated to high pressure like an experiment's, and then the carbonylation chamber was rapidly vented into the decomposition chamber. This simulated the shutdown procedure for

batch experiments. The blow-through experiment showed no powder transfer directly from the carbonylation to the decomposition chamber. This absence of powder transfer supports the theory that iron powder collected in the decomposition chamber was due to the decomposition of iron pentacarbonyl through reaction (3).

The batch process without cooling was done to explore the validity of the apparatus. According to the theory, during the exothermic carbonylation reaction, an increase in temperature and a decrease in pressure due to the CO(g) consumption is expected. This spike in temperature could be prevented, or the external cooling significantly dampens its amplitude. A batch process was run without cooling to check for this expected behavior. During this process, the predicted spike in temperature and decrease in pressure were both visible during experiment E10. After the initial changes, both pressure and temperature leveled off after equilibrium had been reached in a reaction. This supports the observations made in the other batch process experiments and shows that a significant carbonylation reaction occurred in the experiments.

One challenge faced was the seal on the decomposition chamber. Since the vessel was refurbished in-house, no O-rings suppliers could be found. Various seal materials were explored to combat this, including different types of silicones and gasket materials. Given the high temperatures and pressures experienced by these seal materials, many failed due to creep-induced degradation. PTFE is a recommended seal material for future experimentation and application, given its high temperature and pressure applications. An additional risk that was present during the carbonylation experiments was gas leaks. Any leak is hazardous, given the dangerous CO(g) used in the experiments. The system was frequently tested for leaks using pressure checks and leak detection fluid to combat and mitigate this risk. Whenever leaks were discovered, they were fixed before they became a danger.

Due to the late delivery of the reaction vessel and issues with the heating and seal of the decomposition chamber, the number of experiments and the scope of thermodynamic exploration were limited. Additionally, the experiments using continuous flow and their application were not developed due to time constraints. Based on pressure drop and powder collected results, the most successful temperature was 120 °C with 55 bar. Previous thermodynamic calculations support this. Further exploration into varying temperatures and pressures would be needed to create a robust kinetic model. Additional experimentation into controlled continuous flow processes should also be explored, as calculation and simulation show significantly increased yield. The final form of a CIR system and its optimal parameters cannot be concluded from the current data, but this work has proved that using a CIR in situ on the Moon to produce iron from regolith is feasible.

Testing Samples in a Second High-Pressure Reaction System for Results Verification

To control for variables specific to our system, our team sought the assistance of another research group on campus with a High-Pressure wire-mesh Thermogravimetric Apparatus (HTPA). The HTPA comprises a gas supply, pressure control system, heated pressure vessel containing the sample, and microbalance for continual weight measurement. The TGA uses a mesh-type sample holder to enhance the gas/sorbent contact surface in a 0.3 L reaction chamber. The weight percentage change, gas flow rates, pressure, and temperature are recorded throughout the experiment. The system can reach up to 100 bar and 1000 °C with a heating rate of 25 °C/min (Sanna et al., 2022).

Two experiments were performed with 99.5% purity CO(g): A) 55 bar, 120 °C, under 0.2 SLPM flow for a duration of 3 hours 49 minutes; B) 80 bar, 180 °C, under 1.5 SLPM flow for a duration of 3 hours 39 minutes (Figure 11). The experiments begin with settling the microbalance at the specified flow rate. The pressure was increased to the target value once the system stabilized at the desired temperature. The mesh containing ~ 200 mg of Pioneer Astronautics lunar regolith simulant Experiment E8, magnetically concentrated to 24 wt% Fe, was lowered in the reactor into the CO(g) stream.

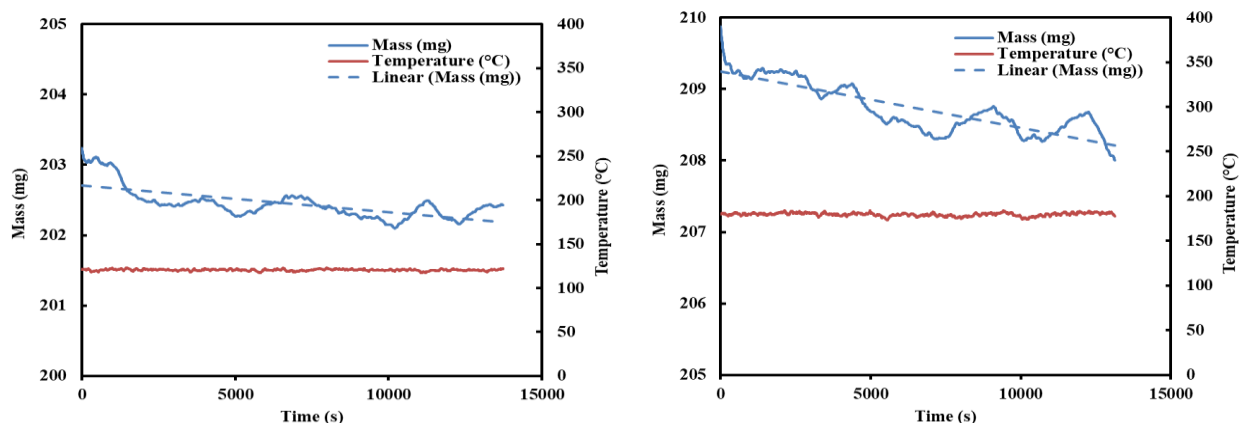


Figure 11: High-Pressure wire-mesh Thermogravimetric Apparatus experiments for:
 A) 55 bar, 120 °C, 0.2 SLPM of CO(g), 3 hours 49 minutes of duration;
 B) 80 bar, 180 °C, 1.5 SLPM of CO(g), 3 hours 39 minutes.

The results indicate a decrease of 0.8 mg in Experiment A (0.4 wt% loss) and 1.9 mg in Experiment B (0.9 wt% loss). If the weight loss is attributable to iron carbonyl formation, this would entail a conversion rate of 1.1 wt% Fe/h. This is slower than anticipated, as the formation rate for Terekhov & Emmanuel was 1.56 wt% Fe/h for the slowest TGA experiment, performed at 180 °C and 60 bar (Terekhov & Emmanuel, 2013). One possible explanation is that the condition of the feed material inhibited the formation rate, as the investigation found as much as a 10-fold difference in formation kinetics depending on whether the material was partially or fully reduced.

It should be noted that another possible source of mass reduction is the formation of Ni(CO)₄(g) from nickel contained in the TGA sample holder (SS316). However, a study suggests that stainless steel may have some resistance to Ni leaching from Ni(CO)₄(g), where Ni loss was 4.9×10^{-6} mg/(h*cm²) at 200 °C and 6.9 MPa, although the gas mixture contained only 51 vol% CO(g) (Inouye & DeVan, 1978).

5.4 Safety Plan and Protocols

An SOP to plan, monitor, and perform experiments has been written, including the HTF, CIR operation, and gas handling system. The documents have been reviewed and approved by the Principal Investigator, Safety Personnel, and Students to ensure safety in the execution of each step.

Safety precautions were taken during the HTF and CIR construction. Testing hazards were reviewed for keeping a safe use of the equipment, where CO(g) and H₂(g) leak tests were conducted using combustible gas detectors and portable/surface-mount detectors. Mitigation plans of constant SOP steps revision, a buddy system, completion of Chemical Hygiene Training and Laboratory Safety Awareness from OEHS, and an emergency response verification were performed.

The risk matrix, risk statement, and closure criteria have been considered according to the consequence and likelihood of occurrence classifications from NASA S3001 Guidelines for Risk Management (NASA, 2017). The consequence options defined are i) Catastrophic (Loss of human life or permanent disability, loss of entire system); ii) Critical (major injury or system damage); iii) Moderate (presence of injury or system damage); iv) Low (minor injury or system damage); v) Negligible (no injury or system damage). The likelihood options defined are i) Near Certainty (event will frequently occur, 80% - 100% probability); ii) Highly Likely (event will occur several times, 60% - 80% probability); iii) Likely (likely to occur sometime, 40% - 60% probability); iv) Low Likelihood (remote possibility of occurrence, 20% - 40% probability); v) Not Likely (very rare, 0% - 20% probability). The consequence and likelihood allow defining the level of exposure as i) Very High; ii) High; iii) Moderate; iv) Minimum; v) None.

6. Results and Conclusions

This project aimed to develop an innovative technology that uses minerals from the lunar regolith to produce steel on the moon. The proposed technology is a novel two-stage process for separating and collecting reduced iron starting from minerals onsite. The testing performed shows that the designed solution does work as intended. However, based on the current results, significant optimization and scale-up considerations exist before the process can hit all of the proposed objectives.

In the reduction stage, the metal oxides in the simulant lunar regolith were reduced by CO(g) gas to yield impure iron metal for the carbonylation and decomposition of iron carbonyl. Eight reduction experiments were run under various conditions. The sample that had the lowest weight loss was the 6-hour sample. This was hypothesized to be due to CO(g) decomposing into C(s) and CO₂(g) through the Boudouard Reaction. A dark deposition on the walls of the ceramic tube, which extended onto part of the surface of the 6-hour sample, supported this conclusion. XRD and XPS confirmed the presence of metallic iron in the samples post-reduction. The highest reduction achieved was ~3.6 wt% Fe after 6 hours under 100% H₂(g) flow. The amount of Ilmenite likely limited this in the lunar regolith sample. There is a difficulty with the Olivine and Pyroxene reduction due to the silica shells and layers.

In the carbonylation and decomposition stage, the system uses pressurized CO(g) to concentrate iron contained in the lunar regolith from the reduction stage into a high-purity fine iron powder via the formation and subsequent decomposition of Fe(CO)₅(g). Eleven successful carbonylation experiments were developed, producing between 2 to 46 mg of iron product powder. The largest amount of powder was 46 mg from experiment E8, which ran at 120 °C and 55 atm for ~410 minutes. This experiment used reduced regolith with ~6.4 wt% Fe from Pioneer Astronautics. For experiment E11 with similar conditions to experiment E8, reduced simulant lunar regolith from the HTF with ~1.37 wt% Fe was used, obtaining an iron powder product. The lower the temperature and the higher the pressure will result in a greater yield, as predicted by thermodynamics. The experimental work supported this fact, as operating at a lower temperature and higher pressure resulted in the greatest amount of iron product. This showed that the CIR system can extract and purify iron using a low initial iron content.

Pycnometer and particle size distribution (Shimadzu SALD-2300) tests were run in the Powder Metallurgy Research Lab managed by Dr. Zhigang Fang. The results are presented in Table III. The final products from the carbonylation experiments in experiments E2 and E5 show different mean particle sizes compared with the Iron Puriss powder and HTF reduction powder. The standard deviation values are less than 0.28.

Table III: Summary of particle size distribution and pycnometer results.

Sample	HTF reduction product powder	Iron Puriss powder	E2 product	E5 product
Mean Particle Size (µm)	297	95	223	213
Density (g/cm ³)	3.17	7.62	3.20	3.48

Experiments were also conducted to verify that the resulting iron powder was not the result of the starting powder being blown through the system. SEM (FEI Quanta 600 FEG) analysis coupled with EDS was used to compare the loaded powder from the carbonylation chamber with the powder collected from the decomposition chamber. Starting powder and product samples considering 120 °C and 55 atm from experiments E3, E8, and E11 were analyzed. Each product revealed product particles different concerning their starting material and of nearly identical particle morphology and composition of ~93 wt% iron and ~7 wt% oxygen between them, as shown in Figures 12 - 14. Each test indicated an oxygen content error of ≤9%, which confirms the assumption that iron was transferred correctly from the carbonylation chamber to the decomposition chamber.

The SEM provided accurate readings of the particle size of each sample, confirming different particle size and morphology characteristics for the initial reactant and final powder product. Figure 12 demonstrates a significant difference in particle size, from 187 μm to 51 μm , a change which was observed across all samples tested as in Figure 13 from 1.04 mm to 85 μm , and in Figure 14 from 730 μm to 199 μm . Such a decrease in particle size was expected due to the low iron concentration, and thus low partial pressure, of iron carbonyl molecules in the decomposition chamber.

Overall, the results of this project show the promise of the novel two-stage process that can separate and collect reduced iron from lunar regolith. Lunar regolith, with as low as 1.37 wt% iron powder, can be used in the CIR process to extract and purify the iron. Verification testing supports that the process can be scaled up and is compatible with other relevant processes.

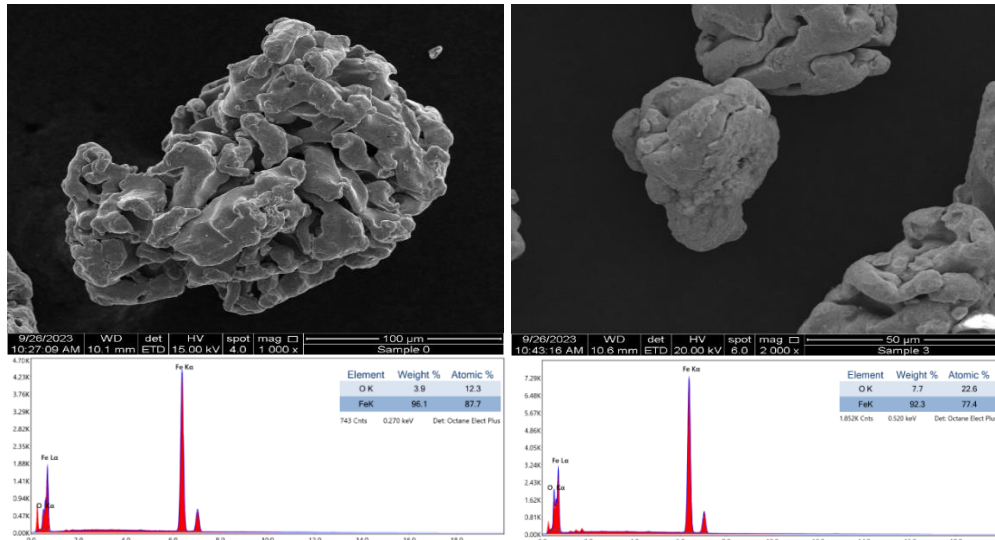


Figure 12: SEM-EDS of A) Synthetic iron puriss powder; B) Iron powder product from experiment E3.

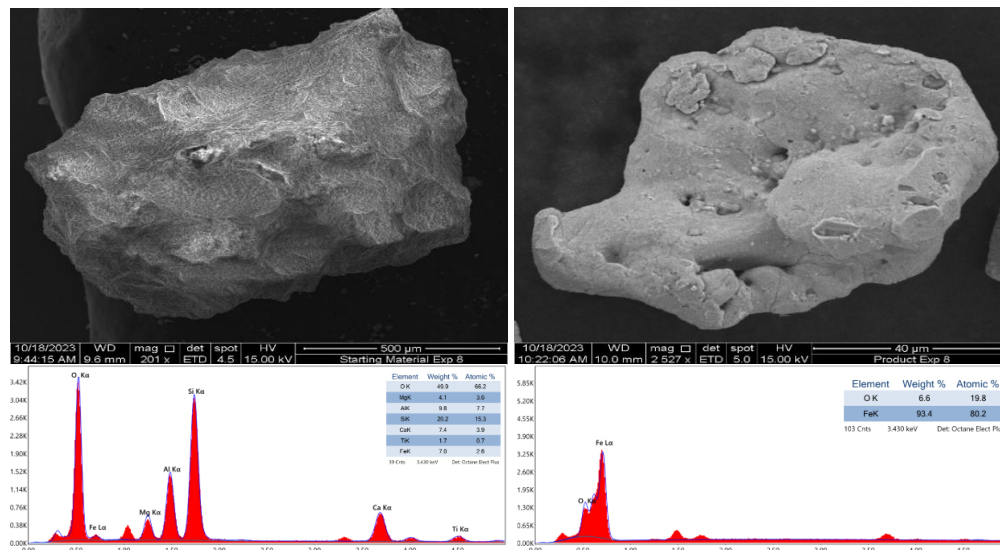


Figure 13: SEM-EDS of A) Lunar Regolith from Pioneer Astronautics; B) Iron powder product from experiment E8.

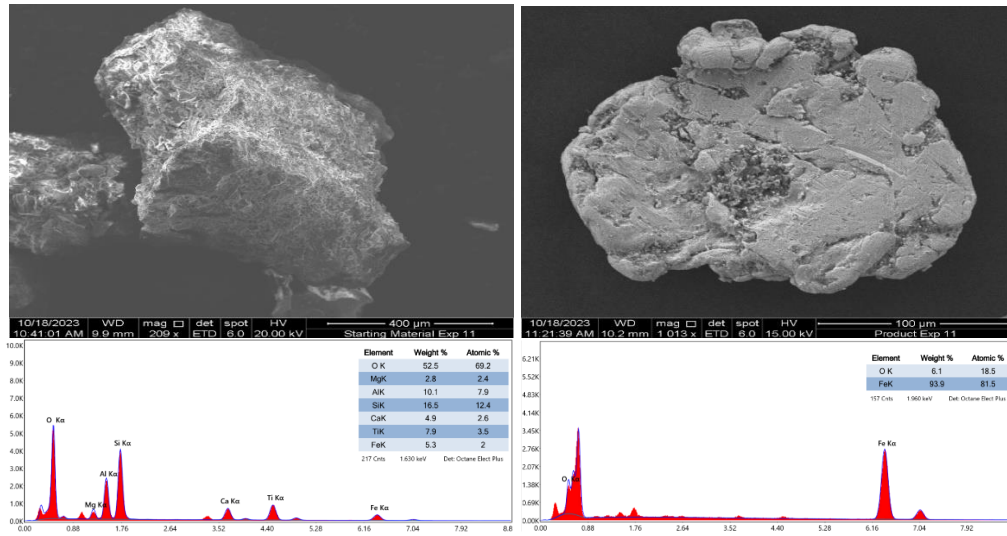


Figure 14: SEM-EDS of A) Sample LR HTF powder starting material; B) Fe product powder experiment E11.

The XRD results (Rigaku Miniflex 600) for Experiment E8 product powder indicate that iron was formed in the decomposition chamber of the carbonylation/decomposition system (Figure 15). Furthermore, no silicon or titanium peaks were identified, which corroborates that there is no blow-through from the carbonylation towards the decomposition chamber and that the iron powder is being formed under the experimental tested conditions. Also, two carbonylation/decomposition experiments with CO(g) were performed using an HPTA, one at 55 bar and 120 °C and one at 80 bar and 180 °C. The results are a decrease of 0.8 mg and 1.9 mg, respectively, indicating that Fe(CO)₅(g) formation is occurring, consistent with the carbonylation and decomposition experiments. However, kinetics would suggest that a more extended investigation must be performed to obtain more significant weight loss.

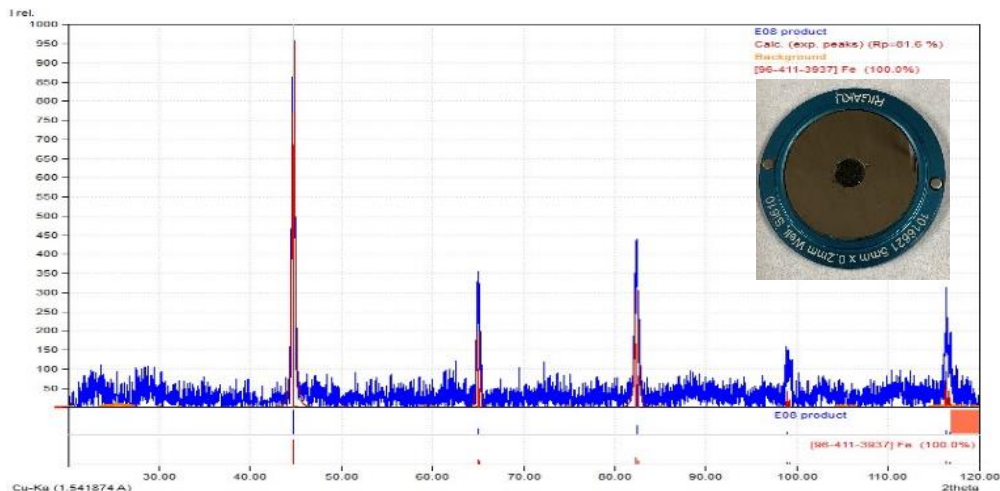


Figure 15: XRD of experiment E8.

The verification testing indicated that the proposed CIR technology could be scaled up for different mission scenarios, increasing the loading weight percentage of iron and reaction time and integrating the interconnected reduction and carbonylation/decomposition continuously. Furthermore, the compatibility with the systems directly preceding and following CIR could be demonstrated. The compatibility was demonstrated by magnetically concentrating and extracting a portion of the reduced iron. The proven compatibility between the two technologies needs to be expanded upon in future research.

7. Path-To-Flight

Several aspects must be considered for the anticipated path-to-flight. Additional experiments would need to be performed to investigate the possibility of increasing iron powder production. These would include the addition of a sulfur catalyst in the carbonylation step, pressure optimization, and altering the current design to allow for continuous flow. The final design would need to be scaled up from the setup used and optimized for lunar conditions.

The small addition of a sulfur or inorganic sulfur compound to act as a catalyst has increased the yield. About a 1 wt% addition of sulfur increased the yield significantly. The yield lowered with greater sulfur additions (Hieber & Geisenberger, 1950). Pioneer Astronautics designed a lunar sulfur capture that can capture over 90% of the sulfur gases emitted from the thermal treatment of lunar soils. That sulfur capture system could be used in conjunction with the system proposed detailed here to limit the hauling of necessary cargo.

Continuous flow, instead of a batch process, would result in a greater yield of iron powder. A mass flow controller would need to be installed into the line before the gas reaches the formation chamber to change the current system to continuous flow. This will ensure the same conditions throughout the entire system. Further experiments to optimize the pressure would also be recommended to maximize the iron powder yield produced.

The reactor's design needs to be scaled up to increase iron powder production. The square cube law suggests that increasing the reactor size would mean reaching the “break-even point” faster, as the reaction volume will increase faster than the heavy parameter of the vessel walls. The quantity of iron produced by the process on Earth (29,000 tons/year from a single facility) supports the assertion that it can be scaled up. However, some practicalities must be taken into consideration. The apparatus must be transferred as a unit, as welds or rivets can act as initiation points for rupture.

In the path-to-flight to the Moon related to critical modifications that would be made to the design for its use onsite, furnace dimensions for iron oxide reduction and pressure vessel dimensions for Fe(s) formation may be considered if a larger production is expected. Also, panels that protect the equipment at all times should be installed onsite to protect it from lunar dust, and withstand adverse circumstances and the lunar environment.

Apollo missions have demonstrated a high risk of dust-related damage, whose impact is increased when performing human exploration and robotic activities. The solar wind can charge lunar dust particles, making them easily get stuck to surfaces and cannot be removed by brushing. The ‘Moon Duster’ is a hand-held electron beam device developed by NASA, in which the repulsive force between negatively charged dust particles ejects them off the surface. This technology could potentially be used on any dust-covered space hardware and would enable the correct operation of the system (NASA-C, 2021).

8. Timeline

The timeline considers the full scope of the research project. A task schedule is divided into different steps, project milestones towards accomplishing the objectives and goals, and deliverables to be presented in specific deadlines are detailed.

8.1 Tasks schedule

The project was divided into five consecutive sections: i) concept development; ii) system design engineering; iii) experimental system; iv) testing, characterization & refining; v) other. Each section consisted of defined tasks contributing to the accomplishment of the results, detailed in Figure 9. Agreed timelines, address challenges, and tasks status by each group member, and periodic meetings were conducted weekly to ensure efficient and effective communication of the project's progress.

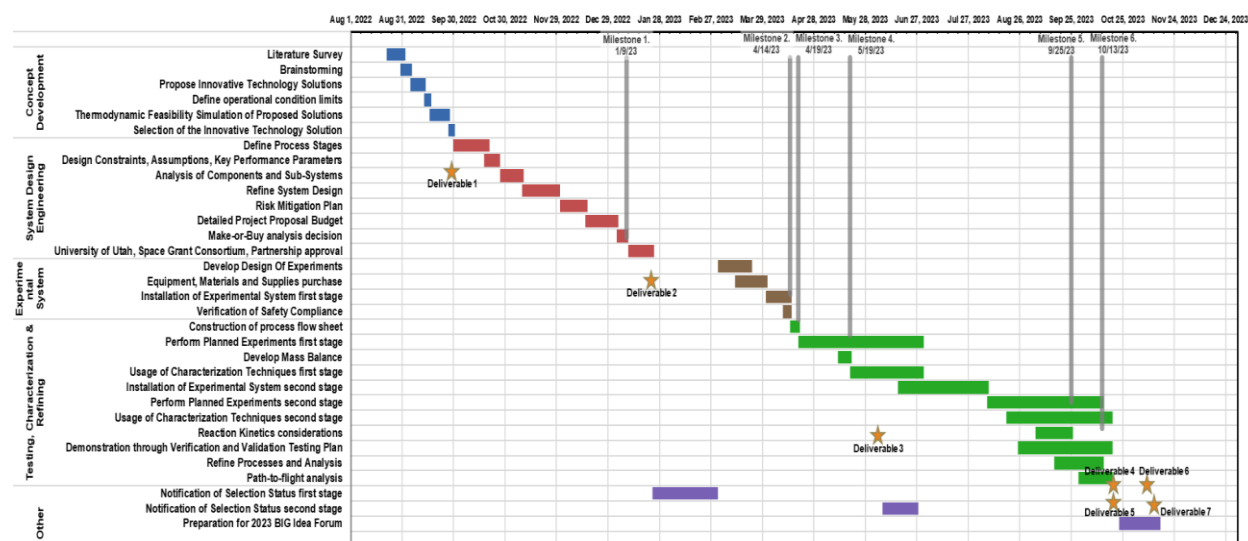


Figure 9: Tasks schedule, milestones, and deliverables summary.

8.2 Project milestones

1. Definition of the Complete System Design (1/9/23)
2. Installation and Commissioning of the Experimental Setup (by 4/14/23)
3. Initial Tests of the Experimental Setup First Stage (4/19/23)
4. Process Simulation Model (5/19/23)
5. Evaluate the Kinetic via Experimental Data (9/25/23)
6. Complete Experimental Runs Second Stage (10/13/23)

8.3 Deliverables

1. Notice of Intent providing a high-level overview of the proposed project concept (9/30/22)
2. Project Proposal and Overview Video that describes the project concept (1/24/23)
3. Mid-Project Report demonstrating the development process (6/7/23)
4. Technology Verification Testing Demonstration (10/23/23)
5. Technical Paper that provides experimental results (10/23/23)
6. Technical Poster and Presentation Chart Deck (11/12/23)
7. 2023 BIG Idea Forum with Poster Session conducted on-site (11/15/23)

9. Budget

The total project expenses considered the costs of direct labor of key personnel and other personnel, fringe benefits, direct costs of equipment and domestic travel, and other direct costs of materials & supplies, testing costs, services, and miscellaneous. The University of Utah indirect costs were waived for Phase I and II, as well as the Space Grant indirect costs for Phase II. The total budget for the project is \$176,310.17, from which \$17,079.82 is the total budget remaining up to 09/30/2023. There are encumbered costs associated with salaries, materials and supplies, and domestic travel to the 2023 BIG Idea Challenge Forum. The total remaining funding will be used in the remaining project time.

Table IV: Summary of budget spent in Phases I and II.

University of Utah
Production of Steel from Lunar Regolith through Carbonyl Iron Refining (CIR)
2023 BIG Idea Challenge

Budget Period of Performance: February 1 - December 31, 2023

Description	Rate	2/1/23 - 6/30/23	Budget Spent	Rate	7/1/23 - 12/31/23	Budget Spent	Total Budget Remaining
A. Direct Labor - Key Personnel							
	0%	\$ 8,936.17	\$ 29,840.60		\$ 26,063.83	\$ 39,964.11	\$ (34,804.71)
<i>Subtotal Salary</i>		\$ 8,936.17	\$ 29,840.60		\$ 26,063.83	\$ 39,964.11	\$ (34,804.71)
Direct Labor - Other Personnel							
	0%	\$ 23,368.09	\$ 15,350.52		\$ 28,931.91	\$ 23,589.30	\$ 13,360.18
<i>Subtotal Other Personnel</i>		\$ 23,368.09	\$ 15,350.52		\$ 28,931.91	\$ 23,589.30	\$ 13,360.18
B. Fringe Benefits							
Faculty	37%	\$ 3,306.38		37%	\$ 9,643.62		\$ 12,950.00
Students	9%	\$ 2,103.13		9%	\$ 2,603.87		\$ 4,707.00
<i>Subtotal Fringe</i>		\$ 5,409.51	\$ 8,702.14		\$ 12,247.49	\$ 12,095.05	\$ (3,140.19)
Total Labor Costs (A+B)		\$ 37,713.77	\$ 53,893.26		\$ 67,243.23	\$ 75,648.46	\$ (24,584.72)
C. Direct Costs - Equipment (any individual item over \$5,000)		\$ 27,710.00	\$ -		\$ -	\$ -	\$ 27,710.00
D. Direct Costs - Domestic Travel		\$ -	\$ -		\$ 14,318.00	\$ 2,060.00	\$ 12,258.00
E. Other Direct Costs							
Materials and Supplies		\$ 16,825.17	\$ 22,790.04		\$ -	\$ 4,905.31	\$ (10,870.18)
Testing Costs or Facilities Rental		\$ -	\$ -		\$ 10,000.00	\$ -	\$ 10,000.00
Consultants		\$ -	\$ -		\$ -	\$ -	\$ -
Services		\$ -	\$ -		\$ 2,500.00	\$ -	\$ 2,500.00
Subcontracts/Subawards		\$ -	\$ -		\$ -	\$ -	\$ -
Miscellaneous		\$ -	\$ (36.63)		\$ -	\$ (30.09)	\$ 66.72
<i>Total Other Direct Costs (E)</i>		\$ 16,825.17	\$ 22,753.41		\$ 12,500.00	\$ 4,875.22	\$ 1,696.54
F. Total Direct Costs (A+B+C+D+E+F)		\$ 82,248.94	\$ 76,646.67		\$ 94,061.23	\$ 82,583.68	\$ 17,079.82
Modified Total Direct Costs, if applicable							\$ -
G.i. University Indirect Costs (Phase I & Phase II)	0%	\$ -	\$ -	0%	\$ -	\$ -	\$ -
G.ii. Space Grant Indirect Costs (Phase II only)				0%	\$ -	\$ -	\$ -
H. Total Direct and Indirect Costs (F+G)		\$ 82,248.94	\$ 76,646.67		\$ 94,061.23	\$ 82,583.68	\$ 17,079.82
<i>% of Total Budget (Phase I should be ~46%; Phase II should be ~54%)</i>		46.65%		53.35%			

10. Acknowledgements

The team thanks the National Institute of Aerospace for organizing NASA's 2023 BIG Idea Challenge Lunar Forge: Producing Metal Products on the Moon, and the Production of Steel from Lunar Regolith through Carbonyl Iron Refining (CIR) project's funding. The team thanks Dr. Kevin Whitty from the University of Utah for supporting the idea development, and Jordan Contreras and Jarom Chamberlain for their initial contribution to this project. Also, we would like to express our gratitude to our industry partner Powder Metallurgy Research Lab, for the advice and assistance with powder analysis.

11. References

- Aerospace America (2021). *Walking on rocket propellant*.
<https://aerospaceamerica.aiaa.org/departments/walking-on-rocket-propellant/>
- Atkinson, N. (2020). *Video shows just how crazy the fuel would look if space rockets were transparent*. ScienceAlert - Universe Today. Retrieved January 6, 2023, from <https://www.sciencealert.com/video-shows-how-we-could-see-propellant-use-if-space-rockets-were-transparent>
- Badescu, V. (2016). *Moon: Prospective Energy and material resources*. Springer.
- Bloemacher, D. (1990). Carbonyl iron powders: Its production and New Developments. *Metal Powder Report*, 45(2), 117–119. [https://doi.org/10.1016/s0026-0657\(10\)80122-5](https://doi.org/10.1016/s0026-0657(10)80122-5)
- Cui, Y. (2015) *Carbonylation of Nickel and Iron from Reduced Oxides and Laterite Ore - Doctorate of Philosophy*. thesis.
- Dewar, J., & Jones, H. O. (1905). The Physical and Chemical Properties of Iron Carbonyl. *Proc. R. Soc. Lond. A*, 76, 558–577. <https://doi.org/10.1098/rspa.1905.0063>
- Ellery, A. (2020). Sustainable in-situ resource utilization on the Moon. *Planetary and Space Science*, 184, 104870. <https://doi.org/10.1016/j.pss.2020.104870>
- Exolith Lab (2023). *Lunar Mare (LMS-1) high-fidelity moon dirt simulant*. Exolith Lab. <https://exolithsimulants.com/collections/regolith-simulants/products/lms-1-lunar-mare-simulant>
- Hieber, W., & Geisenberger, O. (1950). Über metallcarbonyle. XLVII. über den Einfluß von Chalkogenen auf die Entstehung von Eisenpentacarbonyl aus den Komponenten. *Zeitschrift Für Anorganische Chemie*, 262(1–5), 15–24. <https://doi.org/10.1002/zaac.19502620104>
- Inouye, H., & DeVan, J. H. (1978). Formation of Iron Carbonyl between a 1/2% Mo Steel and High-Pressure Gases containing Carbon Monoxide. Tennessee; Oak Ridge National Laboratory.
- Inovar Corporations Ltd. (2017). The Changing Landscape of Carbonyl Iron and Nickel Powder Production. *Powder Metallurgy Review*, 6(1), 43–45.
- Kim, S.-K., Mehran, M. T., Mushtaq, U., Lim, T.-H., Lee, J.-W., Lee, S.-B., Park, S.-J., & Song, R.-H. (2016). Effect of reverse Boudouard reaction catalyst on the performance of solid oxide carbon fuel cells integrated with a dry gasifier. *Energy Conversion and Management*, 130, 119–129. <https://doi.org/10.1016/j.enconman.2016.10.047>
- Korotev, R. L. (2023). *The chemical composition of Lunar Soil*. Earth and Planetary Sciences - Some Meteorite Information. Retrieved January 6, 2023, from <https://sites.wustl.edu/meteorite/items/the-chemical-composition-of-lunar-soil/>
- Landsman, Z. (2020). (rep.). *Exolith Simulants Constituents Report - Exolith Lab*. CLASS Exolith Lab.
- Loff, S., & Dunbar, B. (2019). *Artemis program*. NASA. Retrieved August 31, 2022, from <https://www.nasa.gov/artemisprogram>
- M.A. Balbaa, A. Ghasemi, E. Fereiduni, M.A. Elbestawi, S.D. Jadhav, J.-P. Kruth, “Role of powder particle size on laser powder bed fusion processability of AlSi10mg alloy,” *Additive Manufacturing*, Volume 37, 2021, <https://www.sciencedirect.com/science/article/pii/S2214860420310022>
- Microtrac (2020). *Metal Powders Particle Characterization for Additive Manufacturing*. Microtrac MRB. Retrieved October 19, 2023, from <https://www.microtrac.com/applications/particle-characterization-of-metal-powders/#:~:text=In%20additive%20manufacturing%2C%20the%20particle,cause%20defects%20in%20the%20component.>
- NASA (2020). *Technology readiness levels - NASA earth science and technology office*. Retrieved January 5, 2023, from <https://esto.nasa.gov/trl/>
- NASA (2017). S3001: Guidelines for Risk Management. https://www.nasa.gov/sites/default/files/atoms/files/s3001_guidelines_for_risk_management_-_ver_g_-_10-25-2017.pdf
- NASA (2006). *Magnetic moondust*. NASA. Retrieved January 6, 2023, from https://science.nasa.gov/science-news/science-at-nasa/2006/04apr_magneticmoondust

- NASA-A (2021). *Ideal rocket equation*. NASA. <https://www.grc.nasa.gov/WWW/k-12/rocket/rktpow.html>
- NASA-B (2021). *NASA's plan for sustained lunar exploration and development*. National Aeronautics and Space Administration.
- NASA-C (2021). *New "moon duster" will help clean NASA assets in Space*. NASA Science - Share the Science. Retrieved January 8, 2023, from <https://science.nasa.gov/technology/technology-highlights/new-moon-duster-will-help-clean-nasa-assets-in-space>
- NASA Podcast (2021). *Houston We Have a Podcast Ep 105: Recycling Water and Air*. NASA. Aug. 16, 2019. Retrieved Jan. 10, 2023. <https://www.nasa.gov/johnson/HWHAP/recycling-water-and-air>
- Ponis, S. T. (2021). *Additive Manufacturing and circular economy*. Encyclopedia. Retrieved January 6, 2023, from <https://encyclopedia.pub/entry/10918>
- Roberts, T. G., & Kaplan, S. (2022). *Cost for space launch to low Earth Orbit- Aerospace Security Project*. Aerospace Security. Retrieved January 9, 2023, from <https://aerospace.csis.org/data/space-launch-to-low-earth-orbit-how-much-does-it-cost/>
- Roine, A. (2002). *HSC Chemistry 5.1*; Outokumpu.
- Sanna, A., Thompson, S., Zajac, J. M., & Whitty, K. J. (2022). Evaluation of palm-oil fly ash derived lithium silicate for CO₂ sorption under simulated gasification conditions. *Journal of CO₂ Utilization*, 56, 101826. <https://doi.org/10.1016/j.jcou.2021.101826>
- Shea, G. (2019). *5.3 product verification*. NASA. Retrieved January 5, 2023, from <https://www.nasa.gov/seh/5-3-product-verification>
- Speight, J. G., & Lange, N. A. (2017). *Lange's Handbook of Chemistry*. McGraw-Hill Education.
- Terekhov, D. S., & Emmanuel, N. V. (2013). Direct extraction of nickel and iron from laterite ores using the carbonyl process. *Minerals Engineering*, 54, 124–130. <https://doi.org/10.1016/j.mineng.2013.07.008>

12. Appendix

12.1 Appendix A: Real Gas Law, Fugacity, and Equilibrium Conditions

The Fe(CO)₅(g) critical pressure and temperature is given by (Dewar & Jones, 1905):

$$P_c = 29.6 \text{ atm}$$

$$T_c = 558.15 \text{ K}$$

Calculating Van der Waals constants:

$$\text{volume correction factor} = b = \frac{RT_c}{8P_c} = 0.19342 \frac{\text{L}}{\text{mol}}$$

$$\text{Force constant} = a = \frac{27R^2T_c^2}{64P_c} = 29.899 \frac{\text{L}^2\text{atm}}{\text{mol}^2}$$

The Van der Waals constants of CO(g) are obtained from references (Speight & Lange, 2017). Calculating the compressibility factor of Fe(CO)₅(g) and CO(g) using the Virial equation simplified to the first term with the corresponding fugacity:

$$Z = 1 + \frac{1}{RT} \left(b - \frac{a}{RT} \right) P + \left(\frac{b}{RT} \right)^2 P^2$$

$$f = P * \exp \left[\left(b - \frac{a}{RT} \right) \frac{P}{RT} \right]$$

Free energy of formation

At equilibrium,

$$\Delta G^o = -RT \ln(K) = -RT \ln \left(\frac{a_{\text{Fe(CO)}_5}}{a_{\text{Fe}} * a_{\text{CO}}^5} \right)$$

The activity of a pure solid phase is one:

$$a_{\text{Fe}} = 1$$

The activity of a real gas is:

$$a_i = \frac{f_i}{f_o}$$

$$\Delta G^o = -RT \ln \left(\frac{\frac{f_{\text{Fe(CO)}_5}}{f_o}}{\left(\frac{f_{\text{CO}}}{f_o} \right)^5} \right)$$

$$\Delta G^o = -RT \ln \left(\frac{\frac{n_{\text{IPC}} * RT}{V_g} * \exp \left[\left(b_{\text{IPC}} - \frac{a_{\text{IPC}}}{RT} \right) \frac{n_{\text{IPC}}}{V_g} \right]}{\left(\frac{n_{\text{CO}} * RT}{V_g} * \exp \left[\left(b_{\text{CO}} - \frac{a_{\text{CO}}}{RT} \right) \frac{n_{\text{CO}}}{V_g} \right] \right)^5} \right)$$

Using HSC Software 5.1, the values were given for ΔH , ΔS and were fitted in Excel across the temperature range of interest:

$$\Delta G^o = 566.55 * T(^{\circ}\text{K}) - 169,206$$

$$\left(P + \frac{an^2}{V^2} \right) * (V - nb) = nRT$$

$$\Delta G^o = -RT \ln \left(\frac{P_{\text{Fe(CO)}_5} * \exp \left[\left(b - \frac{a}{RT} \right) \frac{P_{\text{Fe(CO)}_5}}{RT} \right]}{P_{\text{CO}}^5} \right)$$

Using HSC 5.1 the values were given for ΔH , ΔS across the temperature range of interest. The following equation to determine ΔG^o was fitted. ΔG^o is assumed to be independent of pressure.

$$\Delta G^o = 566.55 * T - 169,206$$

$$P_{\text{Fe(CO)}_5} = \frac{n_{\text{IPC}} * RT}{V_g}$$

$$\Delta G^o = -RT \ln \left(\frac{\frac{n_{\text{IPC}} * RT}{V_g} * \exp \left[\left(b_{\text{IPC}} - \frac{a_{\text{IPC}}}{RT} \right) \frac{n_{\text{IPC}}}{V_g} \right]}{\left(\frac{n_{\text{CO}} * RT}{V_g} * \exp \left[\left(b_{\text{CO}} - \frac{a_{\text{CO}}}{RT} \right) \frac{n_{\text{CO}}}{V_g} \right] \right)^5} \right)$$

12.2 Appendix B: Power Consumption

Compressor Power Consumption

$$P_{is} = \frac{\gamma Z R * T_1}{\gamma - 1} * \left[\left(\frac{P_2}{P_1} \right)^{\frac{\gamma-1}{\gamma}} - 1 \right] * Q_m * \frac{1}{\eta}$$

γ = gas isentropic coefficient $CO = 1.4$
Gas compressibility factor = Z

T_1 = temperature of decomposition chamber [K]

T_2 = temperature of formation chamber [K]

P_1 = pressure of decomposition chamber

P_2 = pressure of formation chamber

Q_m = compressor throughput $\left[\frac{kg}{s} \right]$

\dot{V} = volumetric flowrate (Used to find Q_m with the real gas law and molar mass of CO)

η = compressor efficiency (assumed 0.75 for calculations)

Power Consumed Heating gas inbound to Decomposition Chamber

$$P = \dot{Q} = \dot{n} C_p (T_1 - T_2)$$

C_p = heat capacity of CO

\dot{n} = molar flow rate

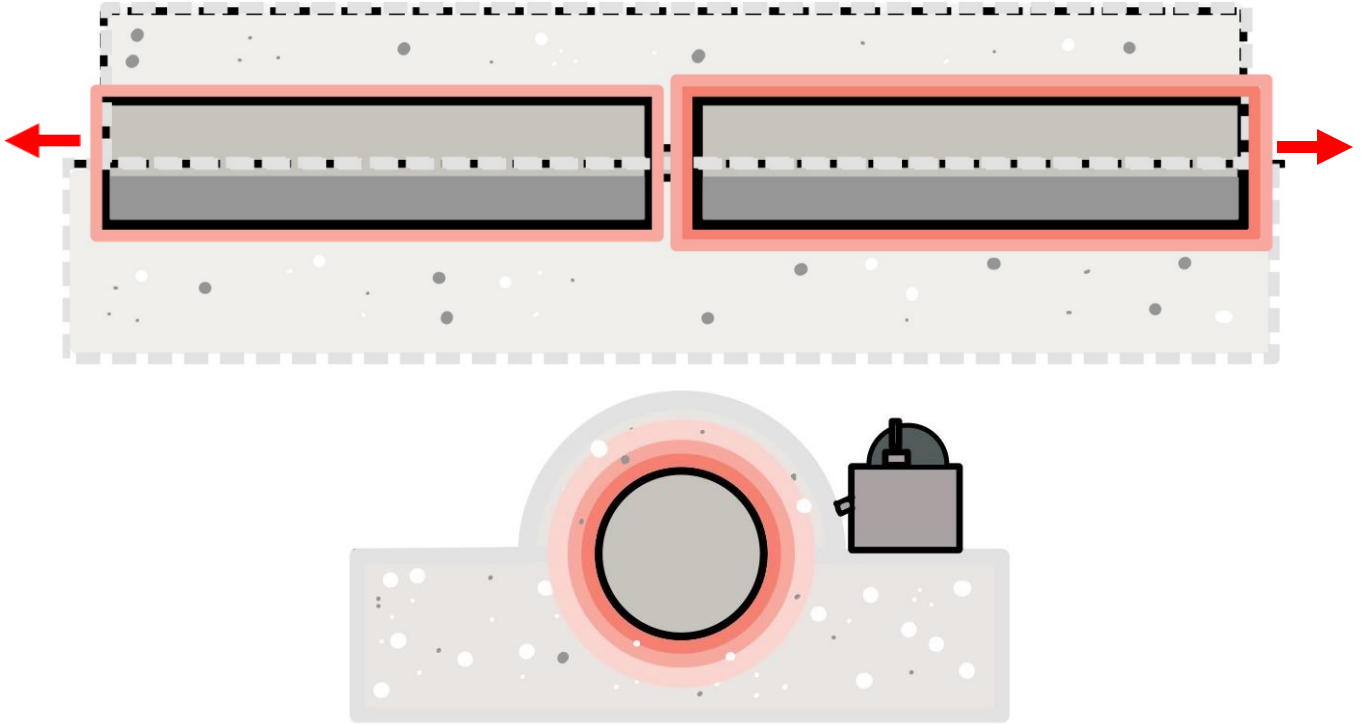
Power Consumed Cooling gas outbound to Formation Chamber

$$P = \dot{Q} = \dot{n} C_p (T_1 - T_2) * \frac{1}{\eta_{cooling}}$$

$\eta_{cooling}$ = cooling system efficiency (assumed 0.9 for calculations)

Power from Heat Losses to the Environment

The apparatus is envisioned to be set in the ground such that surrounding regolith reaches half way up the cylinder walls. Additional regolith is shoveled on top of the two-cylinder chambers to a depth of ~0.5m. The ends of the chambers are dug out and left to allow the chambers to be accessed for regolith regeneration and harvesting of the iron. The compressor and supporting vacuum pump should be sheltered according to their temperature and regolith sensitivities. Heat sinks connecting to the compressor to the outside environment assist the cooling system.



Heat can be simplified as occurring in three primary forms. 1. Heat conducted into the regolith radially from the surface of the chambers; 2. Heat conducted through the titanium tubing and regolith separating the inward faces of the formation and decomposition chambers; 3. Heat radiated from the outward facing exposed chamber ends. Heating and cooling from the compressor and gas line are excluded from this estimate.

1. Radial conduction

A steady state heat transfer is assumed to approximate heat transfer if the rate the temperature of the lunar surface changes throughout the lunar day is sufficiently slow for equilibrium to be maintained. The cylindrical heat transport equation reducing down to $\frac{1}{r} \frac{d}{dr} \left(r \frac{dT}{dr} \right) = 0$, as heat transfer does not occur in the Z direction, defined as passing through the length of the cylinder. As the apparatus is buried within the first meter of regolith, the regolith temperature at relevant depth is assumed to approximate the surface temperature.

Using boundary conditions of $T_i = T_{cylinder}$ when $r_i = R_{cylinder}$ and $T_o = T_{lunar\ surface}$. The heat transfer can be derived to

$$Q = 2\pi r L q_r = \frac{2\pi L k}{\ln\left(\frac{r_o}{r_i}\right)} (T_i - T_o)$$

The radial power consumption will be the contributions from the two cylinders.

$$P = Q_{formation} + Q_{decomposition} = \frac{2\pi L k}{\ln\left(\frac{r_{o,1}}{R}\right)} (T_{formation} - T_o) + \frac{2\pi L k}{\ln\left(\frac{r_{o,2}}{R}\right)} (T_{decomposition} - T_o)$$

For the purposes of estimating power consumption, the experimentally obtained value of the radial distance $r_{o,1}$ and $r_{o,2}$ away from the cylinders to reach $\sim T_o$ is not known and is estimated as $r_{o,1} \approx r_{o,2} = 50 \text{ cm}$.

$$L = \text{cylinder length} = 1.092 \text{ m}$$

$$R = \text{cylinder radius} = 0.1705 \text{ m}$$

$$k = \text{thermal conductivity lunar regolith} \approx 0.8 \frac{\text{W}}{\text{mK}}$$

2. Conduction between the chamber faces

The steady state heat profile between the chambers is due to the temperature difference between them. The energy cost is paid in cooling the formation chamber.

$$Q = A * k * \frac{T_{decomposition} - T_{formation}}{L}$$

$$A = \pi R^2 = 291 \text{ cm}^2 = 0.0291 \text{ m}^2$$

This value is divided up among between regolith that takes up $> 90\%$ of the heat transfer cross section and titanium $< 5\%$ of the cross section.

$$L_1 = \text{short length of Ti gas line between the chambers}$$

$$L_2 = \text{long length of Ti gas line connecting}$$

$$P = A_{regolith} * k_{regolith} * \frac{T_{decomposition} - T_{formation}}{L_1} + A_{Ti} * k_{Ti}$$

$$* (T_{decomposition} - T_{formation}) \left(\frac{1}{L_1} + \frac{1}{L_2} \right)$$

$$k_{Ti} = 17 \frac{\text{W}}{\text{mK}}$$

3. Heat radiated out from the chamber faces

For simplicity, the faces are assumed to be opposite of a flat embankment with the effect of the

$$Q = \varepsilon A \sigma (T_{chamber}^4 - T_{surr}^4)$$

$$\sigma = 5.67 * 10^{-8} \frac{\text{W}}{\text{m}^2 \text{K}^4}$$

$$\varepsilon_{Ti, polished} = 0.3$$

$$P = \varepsilon A \sigma (T_{formation}^4 - T_{surr}^4) + (T_{decomposition}^4 - T_{surr}^4)$$